Redshift evolution of cosmic birefringence in CMB anisotropies

Matteo Galaverni,[1,2,*] Fabio Finelli,[2,3,†] and Daniela Paoletti[2,3,‡]

[1]*Specola Vaticana (Vatican Observatory), V-00120, Vatican City State*
[2]*INAF/OAS Bologna, Via Gobetti 101, I-40129 Bologna, Italy*
[3]*INFN, Sezione di Bologna, Via Irnerio 46, I-40127 Bologna, Italy*

(Received 27 January 2023; accepted 30 March 2023; published 27 April 2023)

We study the imprints of a cosmological redshift-dependent pseudoscalar field ϕ on the rotation of cosmic microwave background (CMB) linear polarization generated by a coupling $\phi F^{\mu\nu}\tilde{F}_{\mu\nu}$. We show how either phenomenological or theoretically motivated redshift dependence of the pseudoscalar field, such as those in models of early dark energy, quintessence, or axionlike dark matter, lead to CMB polarization and temperature-polarization power spectra which exhibit a multipole dependence which goes beyond the widely adopted approximation in which the redshift dependence of the linear polarization angle is neglected. Because of this multipole dependence, the isotropic birefringence effect due to a general coupling $\phi F^{\mu\nu}\tilde{F}_{\mu\nu}$ is not degenerate with a systematic calibration angle uncertainty. By taking this multipole dependence into account, we calculate the parameters of these phenomenological and theoretical redshift dependencies of the pseudoscalar field which can be detected by future CMB polarization experiments on the basis of a χ^2 analysis for a Wishart likelihood. As a final example of our approach, we compute by Markov chain Monte Carlo the minimal coupling g_ϕ in early dark energy which could be detected by future experiments, with or without marginalizing on a systematic rotation angle uncertainty.

DOI: 10.1103/PhysRevD.107.083529

I. INTRODUCTION

When the electromagnetic tensor $F_{\mu\nu}$ is coupled to a pseudoscalar field $\phi(x)$, a new term appears in the Lagrangian density:

$$\mathcal{L} \supset -\frac{g_\phi}{4}\phi F_{\mu\nu}\tilde{F}^{\mu\nu}, \tag{1}$$

where g_ϕ is a model-dependent coupling constant and $\tilde{F}^{\mu\nu} \equiv \frac{1}{2}\epsilon^{\mu\nu\rho\sigma}F_{\rho\sigma}$ is the dual of the electromagnetic tensor. The plane of linear polarization of a single photon propagating in this evolving cosmological pseudoscalar field background undergoes a rotation given by [1,2]

$$\frac{g_\phi}{2}[\phi(x) - \phi(x_{\rm em})], \tag{2}$$

where $\phi(x_{\rm em})$ is the value of the pseudoscalar field when light is emitted. This effect is called *cosmological birefringence*.

First upper limits on the coupling constant g_ϕ were based on optical imaging polarimetry of radio galaxies [2–7]. Soon after, it was realized that cosmic microwave background (CMB) polarization could also be used to study this interaction which induces a rotation of the plane of linear polarization [8–10] to leading order in g_ϕ as well as circular polarization to the next-to-leading order [11,12].

Both the redshift dependence [11,13–18] and the inhomogeneities [18–23] of the cosmological pseudoscalar field contribute to cosmological birefringence. In this paper, we study the imprints of the isotropic redshift dependence of ϕ along the line of sight from the last scattering surface to the observer into CMB parity even and odd power spectra. We consider either phenomenological or theoretically motivated redshift dependence of the pseudoscalar field, such as those in models of early dark energy (EDE), quintessence (DE), or axionlike dark matter (DM) [13,14,24–31].

As already pointed out [11,13,14,16–18], this redshift dependence induces a multipole dependence of the cosmological birefringence effect in the CMB power spectra which goes beyond the widely used approximation for which the rotation angle is assumed constant in redshift [8]. Although this approximation is a key working assumption for deriving constraints from CMB polarization data [32–43] and forecasting the capabilities of future experiments [44–47], we believe it is timely to fully exploit the theoretical predictions of isotropic cosmological birefringence for two main reasons.

First, by assuming the isotropic birefringence angle as independent on the multipoles, an exact degeneracy between the cosmological birefringence effect and the uncertainty in the calibration angle which would be otherwise absent opens

*matteo.galaverni@gmail.com
†fabio.finelli@inaf.it
‡daniela.paoletti@inaf.it

up. We explicitly show how taking into account the redshift dependence of cosmological birefringence mitigate this degeneracy (see also Refs. [16,17]).

As a second point, we stress that the advance in data analysis and in the increasingly precision of CMB polarization data shrank error bars approximately by a factor of 3 from the Planck analysis on data release 2 [36]: Hints of isotropic cosmic birefringence within the constant angle approximation were claimed with Planck data release 3 (DR3) [48], Planck data release 4 (DR4) [49], and more recently with WMAP 9-year and data-processing pipeline called NPIPE [50] ($\alpha = 0.342^{+0.094}_{-0.091}$ deg [51]). For a recent review, see Ref. [52]. We will indeed show that the differences between a physical model and the constant angle approximation are important and within the reach of future CMB polarization experiments.

The paper is organized as follows: In Sec. II, we review the Boltzmann equation in the presence of an isotropic redshift-dependent birefringence. We compare the power spectra for some phenomenological models with the widely used approximation where the time dependence of the linear polarization angle is neglected. The study of theoretically motivated redshift dependence of the pseudoscalar field is presented in Sec. III: early dark energy, quintessence, and axionlike dark matter. In Sec. IV, we present the forecasts for CMB experiments, focusing, in particular, on LiteBIRD on the basis of a χ^2 analysis for a Wishart likelihood, and we perform few exploratory runs exploring the whole cosmological and birefringence parameter space using the Markov chain Monte Carlo code CosmoMC. We conclude in Sec. V.

In this work, we use natural units, $\hbar = c = 1$, and assume flat ΛCDM cosmological model with Planck 2018 estimates of cosmological parameters [53]: $\Omega_b h^2 = 0.02237$, $\Omega_c h^2 = 0.120$, $\tau = 0.0544$, $n_s = 0.9649$, $\ln(10^{10} A_s) = 3.044$, and $H_0 = 100 h\,\mathrm{km\,s^{-1}\,Mpc^{-1}} = 67.36\,\mathrm{km\,s^{-1}\,Mpc^{-1}}$.

II. EFFECTS OF REDSHIFT EVOLUTION OF THE BIREFRINGENCE FIELD

The linear polarization rotation for a CMB photon is described by

$$Q = Q_{\mathrm{rec}} \cos(2\beta) + U_{\mathrm{rec}} \sin(2\beta), \tag{3}$$

$$U = U_{\mathrm{rec}} \cos(2\beta) - Q_{\mathrm{rec}} \sin(2\beta), \tag{4}$$

where Q_{rec} and U_{rec} are the Stokes parameters at recombination, when CMB photons are last scattered.[1]

In the case of an isotropic time-dependent birefringence angle induced by a cosmological pseudoscalar field, the Boltzmann equation for linear polarization contains an additional term proportional to $g_\phi \phi'(\eta)$, where ϕ' is the derivative of ϕ with respect to conformal time η [11,13,14,57]:

$$\begin{aligned}&\Delta'_{Q\pm iU}(k,\eta) + ik\mu \Delta_{Q\pm iU}(k,\eta)\\ &\quad = -n_e \sigma_T a(\eta)\left[\Delta_{Q\pm iU}(k,\eta) + \sum_m \sqrt{\frac{6\pi}{5}}\, {}_{\pm 2}Y_2^m S_P^{(m)}(k,\eta)\right]\\ &\qquad \mp i g_\phi \phi'(\eta) \Delta_{Q\pm iU}(k,\eta).\end{aligned} \tag{5}$$

The cosine of the angle between the CMB photon direction and the Fourier wave vector is indicated by μ, n_e is the number density of free electrons, σ_T is the Thomson cross section, ${}_sY_2^m$ are spherical harmonics with spin weight s, and $S_P^{(m)}(k,\eta)$ is the source term generating linear polarization.

In order to integrate along the line of sight, we note that [14]

$$\begin{aligned}&\Delta'_{Q\pm iU}(k,\eta) + [ik\mu + \tau'(\eta) \pm i g_\phi \phi'(\eta)] \Delta_{Q\pm iU}(k,\eta)\\ &\quad = e^{-ik\mu\eta} e^{\tau(\eta)} e^{\mp i2\alpha(\eta)} \frac{d}{d\eta}\left[e^{ik\mu\eta} e^{-\tau(\eta)} e^{\pm i2\alpha(\eta)} \Delta_{Q\pm iU}(k,\eta)\right],\end{aligned} \tag{6}$$

where we introduced the differential optical depth $\tau'(\eta) \equiv n_e \sigma_T a(\eta)$ and we formally integrated $\phi'(\eta)$ defining $\alpha(\eta) = \frac{g_\phi}{2}\phi(\eta)$, defined up to a constant. Therefore, the Boltzmann Eq. (5) can be rewritten as

$$\begin{aligned}&e^{-ik\mu\eta} e^{\tau(\eta)} e^{\mp i2\alpha(\eta)} \frac{d}{d\eta}\left[e^{ik\mu\eta} e^{-\tau(\eta)} e^{\pm i2\alpha(\eta)} \Delta_{Q\pm iU}(k,\eta)\right]\\ &\quad = -\tau'(\eta) \sum_m \sqrt{\frac{6\pi}{5}}\, {}_{\pm 2}Y_2^m S_P^{(m)}(k,\eta).\end{aligned} \tag{7}$$

Following the integration along the line-of-sight methodology [58], we obtain these expressions for the polarization C_ℓ auto- and cross-spectra:

$$C_\ell^{XY} = (4\pi)^2 \frac{9(\ell+2)!}{16(\ell-2)!} \int k^2 dk [\Delta_{X,\ell}(k,\eta_0) \Delta_{Y,\ell}(k,\eta_0)], \tag{8}$$

$$C_\ell^{TX} = (4\pi)^2 \sqrt{\frac{9(\ell+2)!}{16(\ell-2)!}} \int k^2 dk \Delta_{T,\ell}(k,\eta_0) \Delta_{X,\ell}(k,\eta_0), \tag{9}$$

where X, Y can be either E or B. The integrals defining the polarization scalar perturbations $\Delta_{T,\ell}$, $\Delta_{E,\ell}$, and $\Delta_{B,\ell}$ are, respectively,

[1] We follow CMB-HEALPix coordinate conventions: The linear polarization angle increases clockwise looking toward the source [54–56].

$$\Delta_{T,\ell}(k,\eta_0) = \int_{\eta_{\rm rec}}^{\eta_0} d\eta g(\eta) S_T(k,\eta) j_\ell(k\eta_0 - k\eta), \quad (10)$$

$$\Delta_{E,\ell}(k,\eta_0) = \int_{\eta_{\rm rec}}^{\eta_0} d\eta g(\eta) S_P^{(0)}(k,\eta) \frac{j_\ell(k\eta_0 - k\eta)}{(k\eta_0 - k\eta)^2} \times \cos 2[\alpha(\eta) - \alpha(\eta_0)], \quad (11)$$

$$\Delta_{B,\ell}(k,\eta_0) = \int_{\eta_{\rm rec}}^{\eta_0} d\eta g(\eta) S_P^{(0)}(k,\eta) \frac{j_\ell(k\eta_0 - k\eta)}{(k\eta_0 - k\eta)^2} \times \sin 2[\alpha(\eta) - \alpha(\eta_0)]. \quad (12)$$

Here, $S_T(k,\eta)$ [$S_P^{(0)}(k,\eta)$] is the source term for temperature [scalar polarization] anisotropies, and j_ℓ is the spherical Bessel function of the order of ℓ.

Note that Δ_E and Δ_B are sensitive to cosmic birefringence through a term proportional to $\alpha(\eta) - \alpha(\eta_0)$, where $\alpha(\eta)$ describes linear polarization rotation from recombination ($\eta_{\rm rec}$) to time η:

$$\alpha(\eta) = \int_{\eta_{\rm rec}}^{\eta} \alpha'(\eta_1) d\eta_1. \quad (13)$$

The visibility function $g(\eta) = \tau'(\eta) e^{-\tau(\eta)}$ [58] is not constant for photons propagating from last scattering to nowadays: It reaches its maximum at recombination, and a second peak is present at the reionization epoch, but it is several orders of magnitude smaller. The visibility function of the Boltzmann code CAMB [59] is plotted in Fig. 1 as a function of the redshift.

Since the visibility function is highly peaked at recombination, a widely used approximation consists in evaluating the new term $\alpha(\eta) - \alpha(\eta_0)$ appearing in Eqs. (11) and (12) at recombination [24]. In this approximation,

$$\alpha(\eta) - \alpha(\eta_0) \simeq \alpha(\eta_{\rm rec}) - \alpha(\eta_0) \equiv \bar{\alpha}, \quad (14)$$

the constant terms $\cos(2\bar{\alpha})$ and $\sin(2\bar{\alpha})$ exit integration over time in Eqs. (11) and (12), and the following expressions for the power spectra as a function of the power spectra at recombination (rec) are obtained (assuming at recombination both $C_\ell^{BB,\rm rec} = 0$ and vanishing parity odd power spectra $C_\ell^{TB,\rm rec} = C_\ell^{EB,\rm rec} = 0$) [8,9,14,60,61]:

$$C_\ell^{TE,\rm const} = C_\ell^{TE,\rm rec} \cos(2\bar{\alpha}), \quad (15)$$

$$C_\ell^{TB,\rm const} = C_\ell^{TE,\rm rec} \sin(2\bar{\alpha}), \quad (16)$$

$$C_\ell^{EE,\rm const} = C_\ell^{EE,\rm rec} \cos^2(2\bar{\alpha}), \quad (17)$$

$$C_\ell^{BB,\rm const} = C_\ell^{EE,\rm rec} \sin^2(2\bar{\alpha}), \quad (18)$$

$$C_\ell^{EB,\rm const} = \frac{1}{2} C_\ell^{EE,\rm rec} \sin(4\bar{\alpha}). \quad (19)$$

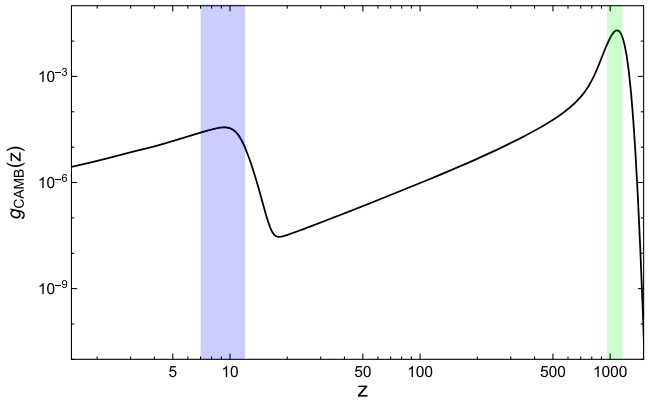

FIG. 1. CAMB visibility function ($g_{\rm CAMB}$) as a function of redshift z; blue band, $7 < z < 12$; green band, $z = z_{\rm rec} \pm 100$ ($z_{\rm rec} \simeq 1059$).

The main purpose of this paper is to compare the results of Eqs. (8) and (9) with the constant approximation of Eqs. (15)–(19).

In order to study in a more detailed way the effects of isotropic cosmic birefringence $\alpha(\eta)$, we modified source terms in the Boltzmann code CAMB [59] following Eqs. (11) and (12). In Fig. 2, we compare the effects on the power spectra of a sudden or instantaneous rotation $\bar{\alpha} = 1$ deg occurring at different epochs. The initial value of the linear polarization angle is always $\alpha(\eta_{\rm rec}) = 0$ deg, and then α drops to -1 deg, but at different epochs. We consider, in particular, $\alpha(\eta) = -1/2\{1 + \tanh[10^4(x - x_*)]\}$ deg, where $x \equiv (\eta - \eta_{\rm rec})/(\eta_0 - \eta_{\rm rec})$ and $x_* = \{0.005, 0.25, 0.5, 0.996\}$. To give an idea of the numbers involved in ΛCDM, we have $x(\eta_{\rm rec}) = 0$, $x(\eta_{z=100}) = 0.08$, $x(\eta_{z=10}) = 0.31$, $x(\eta_{z=5}) = 0.44$, and $x(\eta_0) = 1$. If the change of the linear polarization angle happens nowadays (at $\eta \simeq \eta_0$, or $x_* \simeq 1$), then we clearly have $\alpha(\eta) - \alpha(\eta_0) = 1$ deg during all integration along the line of sight. In this case, the power spectra obtained using the modified Boltzmann code exactly coincide with the analytic expressions in Eqs. (15)–(19) with fixed $\bar{\alpha} = 1$ deg. Note that a miscalibration of the orientation of the detector is assimilable to a rotation at the present time of the linear polarization vector and gives an analog effect on the power spectra [61–63]. We clearly see that the earlier in time the rotation happens, the smaller are the effects on the power spectra (in particular, the difference is larger at lower ℓ). For BB, we also plot the power spectra induced by lensing (black dotted line) and tensor perturbations assuming tensor-to-scalar ratio $r = 10^{-2}$ (dashed black line) and $r = 10^{-3}$ (dot-dashed black line). For a detailed discussion of the impact of lensing on cosmic birefringence, we refer to Ref. [64].

In Fig. 3, we show the output of the modified Boltzmann code considering a rotation $\bar{\alpha}$ of linear polarization (i) localized only at *early times* (from last scattering to reionization)

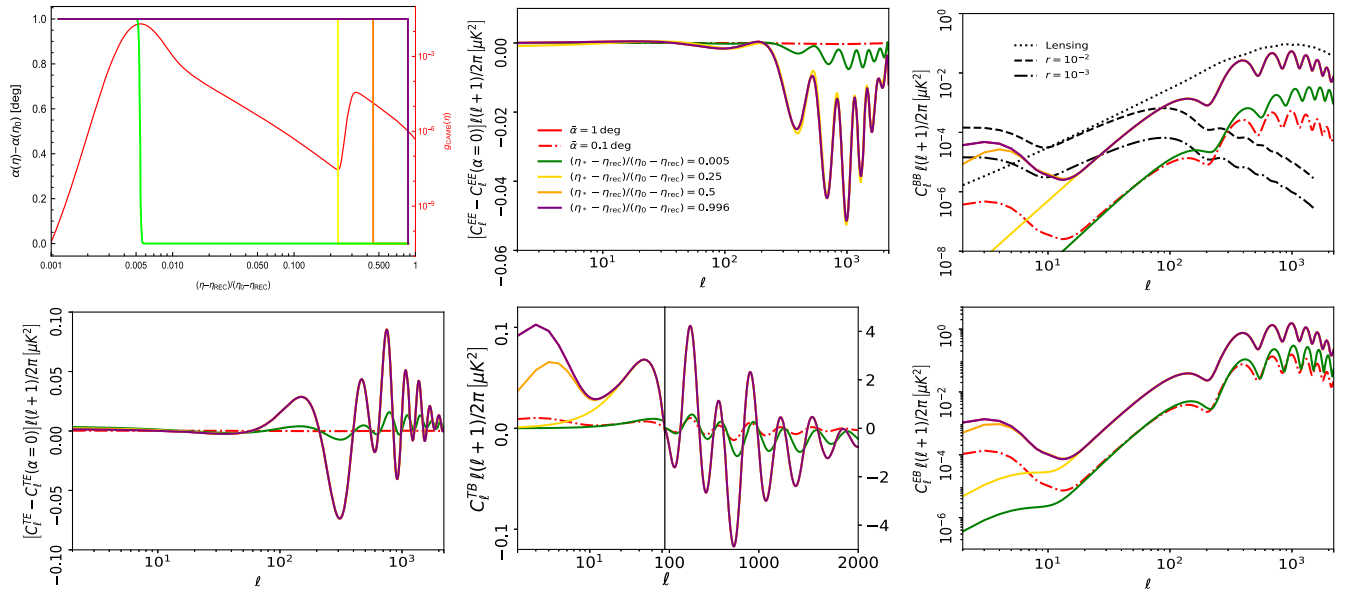

FIG. 2. (a) Evolution of $\alpha(\eta)-\alpha(\eta_0)$ as a function of conformal time $(\eta-\eta_{\rm rec})/(\eta_0-\eta_{\rm rec})$; α always starts at $\alpha(\eta_{\rm rec})=0$ deg and ends at $\alpha(\eta_0)=-1$ deg, but the "sudden or instantaneous rotation" happens at different times: The purple line corresponds to a rotation near present time $x_*\equiv(\eta_*-\eta_{\rm rec})/(\eta_0-\eta_{\rm rec})=0.996$, the orange line corresponds to a rotation occurring at $x_*=0.5$, the yellow line corresponds to a rotation occurring at $x_*=0.25$, and the green line corresponds to a rotation near last scattering surface $x_*=0.005$—the CAMB visibility function $g_{\rm CAMB}$ is plotted in red (on a different scale); angular power spectra obtained with the modified version of CAMB are compared in (b) $C_\ell^{EE}-C_\ell^{EE}(\bar{\alpha}=0)$, (c) C_ℓ^{BB}, where we plot for comparison also the signal induced by gravitational lensing (black dotted line), primordial signal for $r=10^{-2}$ (black dashed line), and primordial signal for $r=10^{-3}$ (black dot-dashed line), (d) $C_\ell^{TE}-C_\ell^{TE}(\bar{\alpha}=0)$, (e) C_ℓ^{TB}, and (f) C_ℓ^{EB}.

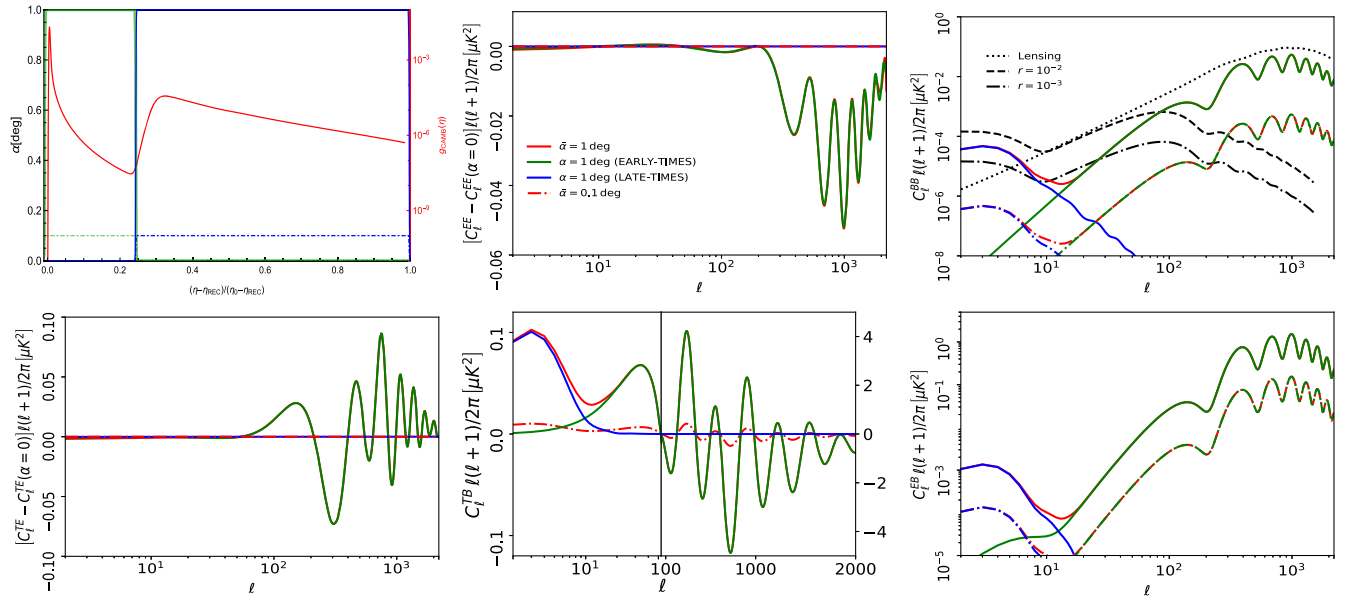

FIG. 3. (a) Evolution of the birefringence angle α as a function of conformal time $(\eta-\eta_{\rm rec})/(\eta_0-\eta_{\rm rec})$: rotation angle equal to 1 deg (0.1 deg) from last scattering to reionization [green continuous (dash-dotted line) line]; rotation angle equal to 1 deg (0.1 deg) from reionization to nowadays [blue continuous (dash-dotted line) line]—the CAMB visibility function $g_{\rm CAMB}$ is plotted in red (on a different scale); angular power spectra obtained with the modified version of CAMB are compared in (b) $C_\ell^{EE}-C_\ell^{EE}(\bar{\alpha}=0)$, (c) C_ℓ^{BB}, (d) $C_\ell^{TE}-C_\ell^{TE}(\bar{\alpha}=0)$, (e) C_ℓ^{TB}, and (f) C_ℓ^{EB}.

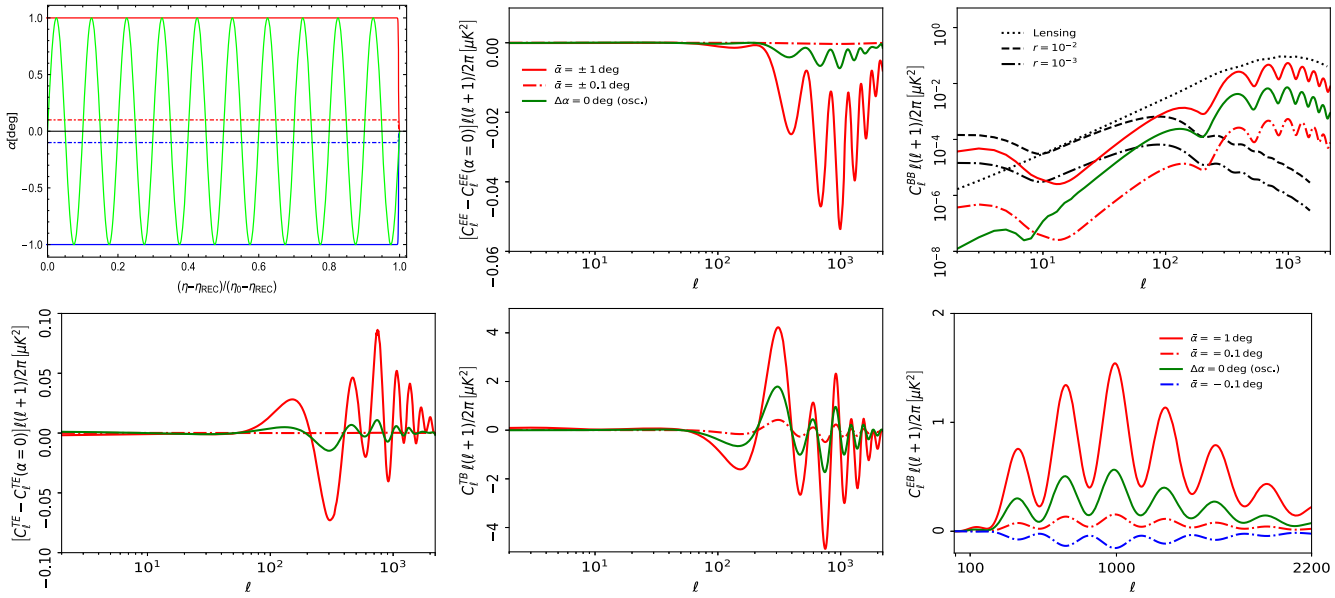

FIG. 4. (a) Oscillating birefringence angle with $\bar{\alpha} \equiv \alpha(\eta_{\rm rec}) - \alpha(\eta_0) = 0$ deg—the linear polarization angle oscillates between 1 and −1 deg: $\alpha(\eta) = \sin(20\pi x)$ (green line); we plot for comparison also the case of a sudden rotation of ± deg (±0.1 deg) occurring at the present time—see the continuous (dot-dashed) red and blue lines. (b) $C_\ell^{EE} - C_\ell^{EE}(\bar{\alpha} = 0)$, (c) C_ℓ^{BB}, (d) $C_\ell^{TE} - C_\ell^{TE}(\bar{\alpha} = 0)$, (e) C_ℓ^{TB}, and (f) C_ℓ^{EB}.

$$\alpha(\eta) = \bar{\alpha}\left\{\frac{\tanh[10^4(x-0.001)]+1}{2} - \frac{\tanh[10^4(x-0.25)]+1}{2}\right\}$$

or (ii) only at *late times* (from reionization to nowadays)

$$\alpha(\eta) = \bar{\alpha}\left\{\frac{\tanh[10^4(x-0.25)]+1}{2} - \frac{\tanh[10^4(x-0.996)]+1}{2}\right\}.$$

Since the linear polarization rotation is not constant over time, the effects on the power spectra are different. If α is rotated only at early times the effects on the power spectra are localized at $\ell \gtrsim 10$. Otherwise, if the linear polarization angle rotates after reionization (late times), the effects are visible only at $\ell \lesssim 10$.

Interestingly, we stress that birefringence effects on the power spectra can be present even if $\alpha(\eta_{\rm rec}) = \alpha(\eta_0)$, differently from what is stated in Ref. [29]. In this case, according to the analytic expressions in Eqs. (15)–(19), there should be no effects, since $\bar{\alpha} = 0$. On the contrary, there are evident effects on the power spectra using the modified CAMB code based on the Boltzmann equation for cosmic birefringence; see, in particular, Fig. 4. See also the Appendix for other interesting phenomenological cases with $\alpha(\eta_{\rm rec}) = \alpha(\eta_0)$.

III. THEORY MODELING

In an expanding universe, a spatially homogeneous scalar field obeys

$$\ddot{\phi} + 3H\dot{\phi} - \frac{dV}{d\phi} = 0, \tag{20}$$

where the overdot denotes derivative respect to cosmic time t. In this section, we specify the potential $V(\phi)$ for (a) axionlike early dark energy (Sec. III A), (b) quintessence (Sec. III B), and (c) axionlike dark matter (Sec. III C). From the evolution of $\phi(t)$, we estimate the effects on CMB power spectra using a modified version of CAMB [59].

A. Axionlike as early dark energy

Early dark energy was proposed in order to solve the tension between the local and the cosmological measurements of the Hubble parameter [27,30,31,65,66]. In this case, we consider a potential of the form

$$V(\phi) = \Lambda^4\left(1 - \cos\frac{\phi}{f}\right)^n, \tag{21}$$

describing the spontaneous breaking of a continuous symmetry at scale f. The evolution of the pseudoscalar field ϕ is determined by the following system of equations:

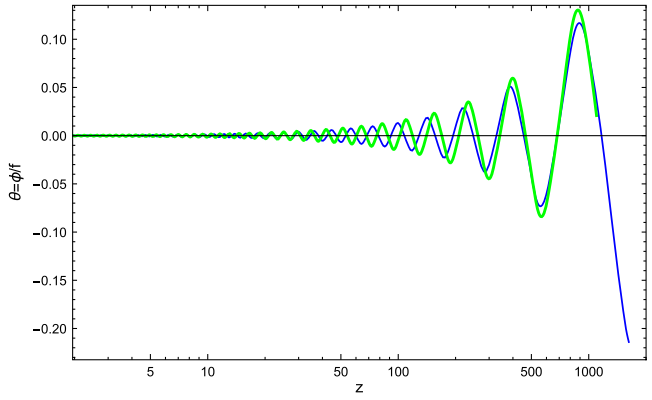

FIG. 5. Early dark energy, evolution of Θ as a function of z from recombination to nowadays for fixed $n = 2$, $\Lambda = 0.417$ eV, $f = 0.05 M_{\rm pl} = 1.22 \times 10^{17}$ GeV, $\Theta_i = 1$, and $\dot{\Theta}_i = 0$: numerical fit of Eq. (24) (green line) and the evolution provided by CAMB-1.3.2 (blue line); in this version of CAMB, EDE is implemented following Ref. [71].

$$\ddot{\phi} + 3H\dot{\phi} + \frac{n\Lambda^4}{f}\left(1 - \cos\frac{\phi}{f}\right)^{n-1} \sin\frac{\phi}{f} = 0,$$
$$H^2 = \frac{1}{3M_{\rm pl}^2}(\rho_{\rm RAD} + \rho_{\rm MAT} + \rho_\Lambda + \rho_\phi), \tag{22}$$

where $M_{\rm pl} = 2.43 \times 10^{18}$ GeV is the reduced Planck mass. Initially, the field is frozen and acts as a cosmological constant, and it begins to oscillate when the effective mass becomes of the order of H. In practice, we solve numerically this system in the new variable $x \equiv \ln t/t_i$, from a fixed point t_i in the radiation-dominated era to nowadays (t_0):

$$\frac{d\Theta}{dx^2} + \left(\frac{3}{a}\frac{da}{dx} - 1\right)\frac{d\Theta}{dx} t_i^2 e^{2x} \frac{n\Lambda^4}{f^2}(1 - \cos\Theta)^{n-1} \sin\Theta = 0,$$
$$\frac{da}{dx} = t_i e^x H_i a \left[\Omega_{\rm RAD,i}\left(\frac{a_i}{a}\right)^4 + \Omega_{\rm MAT,i}\left(\frac{a_i}{a}\right)^3 + \Omega_{\Lambda,i} + \frac{1}{6}\frac{f^2}{H_i^2 M_{\rm pl}^2 t_i^2} e^{-2x}\left(\frac{d\Theta}{dx}\right)^2 + \frac{1}{3}\frac{\Lambda^4}{H_i^2 M_{\rm pl}^2}(1 - \cos\Theta)^n\right]^{1/2}, \tag{23}$$

where $\Theta(t) \equiv \phi(t)/f$. In the oscillating regime, for $n = 2$, we approximate the evolution of Θ as a function of cosmic time with an elliptic sine (sn); see Refs. [67–69]. In particular, for fixed $\Lambda = 0.417$ eV, $f = 0.05 M_{\rm pl} = 1.22 \times 10^{17}$ GeV, $\Theta_i = 1$, and $\dot{\Theta}_i = 0$, the following numerical fit for Θ is obtained [70]:

$$\Theta(\eta) \simeq \left(-6.49 \times 10^{-3} + 2.15 \times 10^{-3}\frac{\eta_0}{\eta}\right) * \mathrm{sn}\left(6.35 \times 10^{-1} + 5.18 \times 10^2 \frac{\eta}{\eta_0}, \frac{1}{\sqrt{2}}\right). \tag{24}$$

In Fig. 5, we plot this function for Θ as a function of redshift z, from recombination to $z = 0$.

In Fig. 6, we plot the power spectra using the evolution of $\Theta(\eta)$ directly provided by the CAMB code. Note that

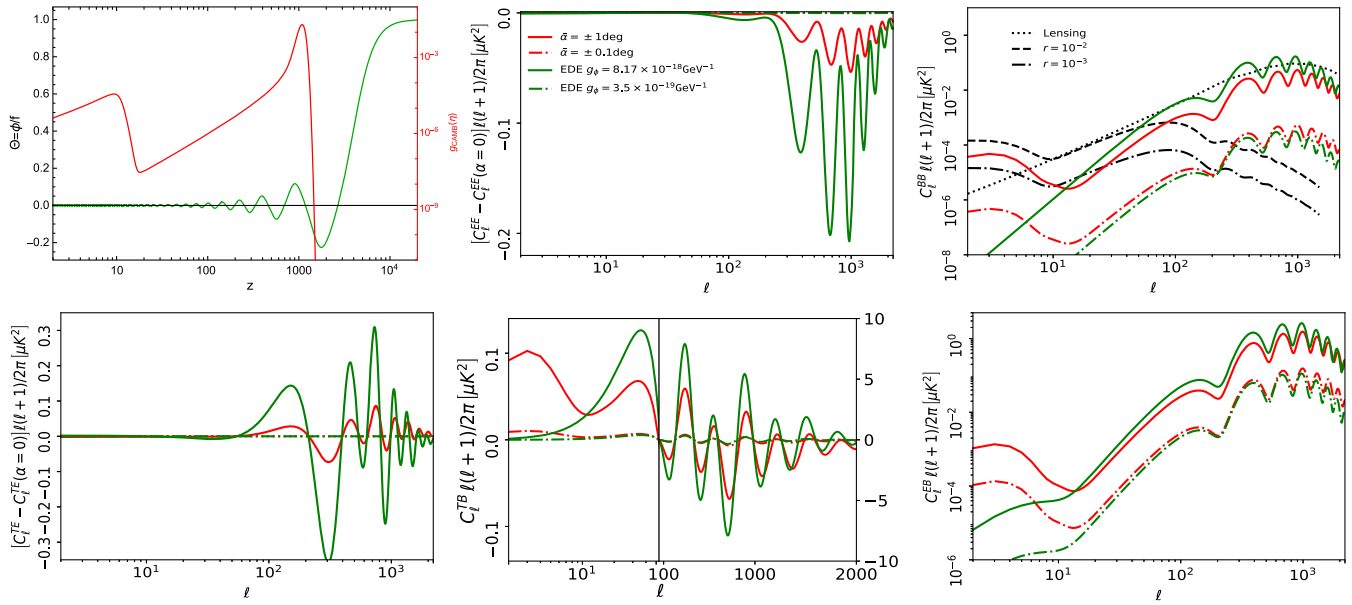

FIG. 6. Early dark energy: (a) evolution for $\Theta \equiv \phi/f$ as a function of the redshift (green line) provided by the code CAMB for fixed $n = 2$, $\Lambda = 0.417$ eV, $f = 0.05 M_{\rm pl} = 1.22 \times 10^{17}$ GeV, $\Theta_i = 1$, and $\dot{\Theta}_i = 0$; the CAMB visibility function $g_{\rm CAMP}$ is plotted in red (on a different scale). Assuming $g_\phi = 8.17 \times 10^{-18}$ GeV^{-1} or $g_\phi = 3.5 \times 10^{-19}$ GeV^{-1}, we plot the angular power spectra for (b) $C_\ell^{EE} - C_\ell^{EE}(\bar{\alpha} = 0)$, (c) C_ℓ^{BB}, (d) $C_\ell^{TE} - C_\ell^{TE}(\bar{\alpha} = 0)$, (e) C_ℓ^{TB}, and (f) C_ℓ^{EB}.

for this model $\Theta(\eta_0)$ is negligible compared to the values at $\eta_{\rm rec}$, since the field is quickly oscillating at $z = 0$. We consider two values of the coupling constant: $g_\phi = 8.17 \times 10^{-18}\ \mathrm{GeV}^{-1}$—corresponding to $\bar{\alpha} = 1.15$ deg—and $g_\phi = 3.5 \times 10^{-19}\ \mathrm{GeV}^{-1}$—corresponding to $\bar{\alpha} = 0.05$ deg. For EE and TE we decided to plot the difference with the standard unrotated spectra, $C_\ell^{EE} - C_\ell^{EE}(\bar{\alpha} = 0)$ and $C_\ell^{TE} - C_\ell^{TE}(\bar{\alpha} = 0)$, in order to underline the differences.

B. Axionlike as dark energy

We consider dark energy driven by an axionlike pseudoscalar, as suggested in Ref. [72], with a potential:

$$V(\phi) = M^4\left(1 + \cos\frac{\phi}{f}\right). \tag{25}$$

We solve numerically the system in the new variable x, as in the previous subsection:

$$\frac{d\Theta}{dx^2} + \left(\frac{3}{a}\frac{da}{dx} - 1\right)\frac{d\Theta}{dx} - t_i^2 e^{2x}\frac{M^4}{f^2}\sin\Theta = 0,$$

$$\frac{da}{dx} = t_i e^x H_i a\left[\Omega_{\mathrm{RAD,i}}\left(\frac{a_i}{a}\right)^4 + \Omega_{\mathrm{MAT,i}}\left(\frac{a_i}{a}\right)^3 + \frac{1}{6}\frac{f^2}{H_i^2 M_{\rm pl}^2 t_i^2}e^{-2x}\left(\frac{d\Theta}{dx}\right)^2 + \frac{1}{3}\frac{M^4}{H_i^2 M_{\rm pl}^2}(1 + \cos\Theta)\right]^{1/2}.$$

For $M \sim 10^{-3}$ eV and $f \lesssim M_{\rm pl}$, the pseudoscalar field mimics the cosmological constant contribution. There are indications from string theory that f cannot be larger than $M_{\rm pl}$ [73,74]. In the future, when the expansion rate of the Universe becomes smaller, the field will start to oscillate and the Universe will become cold dark matter dominated.

The pseudoscalar field became dynamical only recently. By fixing $M = 1.95 \times 10^{-3}$ eV, $f = 0.265 M_{\rm pl}$, $\Theta_i = 0.25$, and $\dot{\Theta}_i = 0$, we use the following numerical fit for $\Theta(\eta)$:

$$\Theta(\eta) \simeq 0.25 + 1.468 \times 10^{-4}\exp\left[8.857\left(\frac{\eta - \eta_{\rm rec}}{\eta_0 - \eta_{\rm rec}}\right)\right]. \tag{26}$$

Differently from the early dark energy model, discussed in the previous subsection, here the field is not oscillating at $z = 0$ and it is important to consider $\Theta(\eta_0)$. Using this numerical fit, we evaluate the linear polarization angular power spectra for $g_\phi = 1.8 \times 10^{-20}\ \mathrm{GeV}^{-1}$, corresponding to a total rotation angle today $\alpha(\eta_0) = 0.35$ deg. In some models, the coupling constant between the pseudoscalar field is assumed to be proportional to the inverse of the energy breaking scale f [75,76]:

$$\mathcal{L} \supset -\frac{C\alpha_{\rm EM}}{2\pi f}\phi F_{\mu\nu}\tilde{F}^{\mu\nu}, \tag{27}$$

where $C \simeq \mathcal{O}(1)$ is a model-dependent constant. Therefore, we discuss also the case $g_\phi = \frac{2\alpha_{\rm EM}}{f\pi} \simeq 7.2 \times 10^{-21}\ \mathrm{GeV}^{-1}$—corresponding to $\alpha(\eta_0) = 0.14$ deg.

See Fig. 7 for the power spectra $C_\ell^{EE} - C_\ell^{EE}(\bar{\alpha} = 0)$, C_ℓ^{BB}, $C_\ell^{TE} - C_\ell^{TE}(\bar{\alpha} = 0)$, C_ℓ^{TB}, and C_ℓ^{EB} evaluated using CAMB.

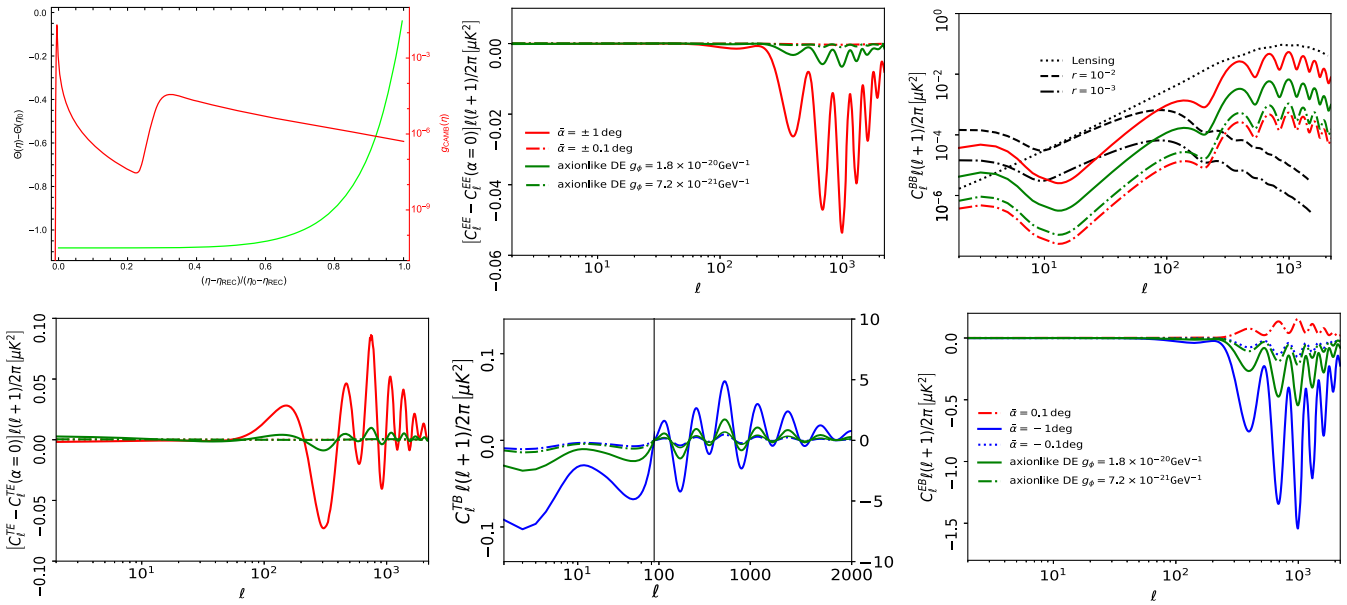

FIG. 7. Axionlike dark energy: (a) evolution of $\Theta(\eta) - \Theta(\eta_0)$ as a function of conformal time $(\eta - \eta_{\rm rec})/(\eta_0 - \eta_{\rm rec})$ is plotted in green at fixed $M = 1.95 \times 10^{-3}$ eV, $f = 0.265 M_{\rm pl}$, $\Theta_i = 0.25$, and $\dot{\Theta}_i = 0$; the CAMB visibility function $g_{\rm CAMB}$ is plotted in red (on a different scale). Assuming $g_\phi = 1.8 \times 10^{-20}\ \mathrm{GeV}^{-1}$ and $g_\phi = \frac{2\alpha_{\rm EM}}{f\pi} \simeq 7.2 \times 10^{-21}\ \mathrm{GeV}^{-1}$, we plot the angular power spectra for (b) $C_\ell^{EE} - C_\ell^{EE}(\bar{\alpha} = 0)$, (c) C_ℓ^{BB}, (d) $C_\ell^{TE} - C_\ell^{TE}(\bar{\alpha} = 0)$, (e) C_ℓ^{TB}, and (f) C_ℓ^{EB}.

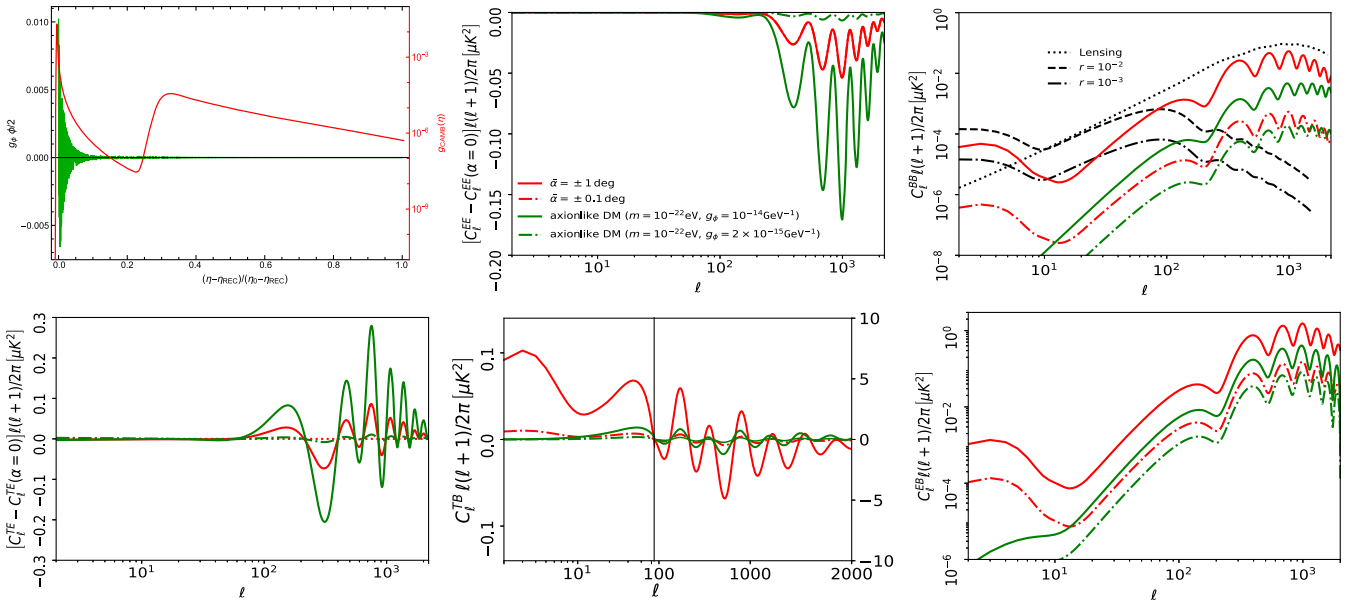

FIG. 8. Axionlike dark matter: (a) evolution of $g_\phi\phi(\eta)/2$ is plotted in green as a function of conformal time $(\eta-\eta_{\rm rec})/(\eta_0-\eta_{\rm rec})$ ar fixed $m = 10^{-22}$ eV and $g_\phi = 10^{-14}$ GeV^{-1} (green continuous line); the CAMB visibility function $g_{\rm CAMB}$ is plotted in red (on a different scale). Assuming $g_\phi = 10^{-14}$ GeV^{-1} (green continuous line) and $g_\phi = 2\times10^{-15}$ GeV^{-1} (light green dashed line), we plot the angular power spectra for (b) $C_\ell^{EE} - C_\ell^{EE}(\bar{\alpha}=0)$, (c) C_ℓ^{BB}, (d) $C_\ell^{TE} - C_\ell^{TE}(\bar{\alpha}=0)$, (e) C_ℓ^{TB}, and (f) C_ℓ^{EB}.

C. Axionlike as dark matter

For an axionlike field acting as dark matter [76–78], we consider the potential

$$V(\phi) = m^2\frac{f^2}{N^2}\left(1-\cos\frac{\phi N}{f}\right), \tag{28}$$

in the regime where the pseudoscalar field oscillates near the minimum. The field evolves according to [11,79]

$$\phi(t) = \sqrt{6\Omega_{\rm MAT}}\frac{H_0 M_{\rm pl}}{m a^{3/2}(t)} \times \sin\left[mt\sqrt{1-(1-\Omega_{\rm MAT})\left(\frac{3H_0}{2m}\right)^2}\right], \tag{29}$$

where the evolution of the scale factor is [80]

$$a(t) = \left(\frac{\Omega_{\rm MAT}}{1-\Omega_{\rm MAT}}\right)^{\frac{1}{3}}\left[\sinh\left(\frac{3}{2}\sqrt{1-\Omega_{\rm MAT}}H_0 t\right)\right]^{\frac{2}{3}}. \tag{30}$$

Since the Boltzmann CAMB code works in conformal time, we fit numerically the relation between cosmic and conformal time from recombination to today; for the ΛCDM cosmological model with Planck 2018 estimates of cosmological parameters, we obtain [53]

$$t \simeq \frac{\eta_0}{3.5041}\left(\frac{\eta}{\eta_0}\right)^{3.09358}. \tag{31}$$

As in the early dark energy case, the field quickly oscillates at $z = 0$; therefore, we can assume $\phi(\eta_0) \simeq 0$. We plot $g_\phi\phi(\eta)/2$ as a function of the time chosen, a particular value for $m = 10^{-22}$ eV and $g_\phi = 10^{-14}$ GeV^{-1}; see Fig. 8(a). Once the source terms for scalar perturbations in the Boltzmann code are modified by inserting the new terms proportional to $\alpha(\eta)-\alpha(\eta_0)$ [see Eqs. (11) and (12)], the rotated power spectra are obtained. In Fig. 8, we plot $C_\ell^{EE} - C_\ell^{EE}(\bar{\alpha}=0)$, C_ℓ^{BB}, $C_\ell^{TE} - C_\ell^{TE}(\bar{\alpha}=0)$, C_ℓ^{TB}, and C_ℓ^{EB} for $m = 10^{-22}$ eV and for two different values of the coupling constant: $g_\phi = 10^{-14}\,\text{GeV}^{-1}$—corresponding to total rotation angle $\alpha(\eta_0) = 0.52$ deg—and $g_\phi = 2\times10^{-15}\,\text{GeV}^{-1}$—corresponding to total rotation angle $\alpha(\eta_0) = 0.103$ deg.

IV. CURRENT MEASUREMENTS AND FORECASTS FOR FUTURE EXPERIMENTS

In this section, we discuss the status of current measurements and forecast the science capabilities of future experiments in the context of cosmological birefringence. We will analyze various cosmological models with different approximations by providing effective $\Delta\chi^2$ and posterior probabilities for parameters by Monte Carlo Markov chain (MCMC) exploration.

The parity-violating nature of the interaction generates nonzero parity-odd correlators (C_ℓ^{TB} and C_ℓ^{EB}). We therefore consider the full theoretical data covariance matrix:

$$\bar{\mathbf{C}}_l = \begin{pmatrix} \bar{C}_\ell^{TT} & \bar{C}_\ell^{TE} & \bar{C}_\ell^{TB} \\ \bar{C}_\ell^{TE} & \bar{C}_\ell^{EE} & \bar{C}_\ell^{EB} \\ \bar{C}_\ell^{TB} & \bar{C}_\ell^{EB} & \bar{C}_\ell^{BB} \end{pmatrix} = \begin{pmatrix} C_\ell^{TT} + N_\ell^{TT} & C_\ell^{TE} & C_\ell^{TB} \\ C_\ell^{TE} & C_\ell^{EE} + N_\ell^{EE} & C_\ell^{EB} \\ C_\ell^{TB} & C_\ell^{EB} & C_\ell^{BB} + N_\ell^{BB} \end{pmatrix}. \quad (32)$$

The noise power spectra are obtained by considering an inverse-variance weighted sum of the noise sensitivity convolved with a Gaussian beam window function for each frequency channel ν [81]:

$$N_\ell^{XX} = \left[\sum_\nu \frac{1}{N_{l\nu}^{XX}}\right]^{-1}, \quad (33)$$

with

$$N_{l\nu}^{XX} = \Delta_{X\nu}^2 \exp\left[l(l+1)\frac{\theta_{\mathrm{FWHM}\nu}^2}{8\ln 2}\right], \quad (34)$$

where $X = \{T, E, B\}$, $\Delta_{X\nu}$ is the detector noise level, and $\theta_{\mathrm{FWHM}\nu}$ is the full width half maximum (FWHM) for a given frequency channel ν.

Following Refs. [82–84], we consider a Wishart likelihood and introduce the effective χ^2_{eff}:

$$\chi^2_{\mathrm{eff}} = \sum_\ell (2\ell+1) f_{\mathrm{sky}}\left(\frac{A}{|\bar{C}|} + \ln\frac{|\bar{C}|}{|\hat{C}|} - 3\right), \quad (35)$$

where f_{sky} denotes the observed fraction of the sky, A is defined as

$$\begin{aligned} A = {} & \hat{C}_\ell^{TT}(\bar{C}_\ell^{EE}\bar{C}_\ell^{BB} - (\bar{C}_\ell^{EB})^2) + \hat{C}_\ell^{TE}(\bar{C}_\ell^{TB}\bar{C}_\ell^{EB} - \bar{C}_\ell^{TE}\bar{C}_\ell^{BB}) + \hat{C}_\ell^{TB}(\bar{C}_\ell^{TE}\bar{C}_\ell^{EB} - \bar{C}_\ell^{TB}\bar{C}_\ell^{EE}) \\ & + \hat{C}_\ell^{TE}(\bar{C}_\ell^{TB}\bar{C}_\ell^{EB} - \bar{C}_\ell^{TE}\bar{C}_\ell^{BB}) + \hat{C}_\ell^{EE}(\bar{C}_\ell^{TT}\bar{C}_\ell^{BB} - (\bar{C}_\ell^{TB})^2) + \hat{C}_\ell^{EB}(\bar{C}_\ell^{TE}\bar{C}_\ell^{TB} - \bar{C}_\ell^{TT}\bar{C}_\ell^{EB}) \\ & + \hat{C}_\ell^{TB}(\bar{C}_\ell^{TE}\bar{C}_\ell^{EB} - \bar{C}_\ell^{EE}\bar{C}_\ell^{TB}) + \hat{C}_\ell^{EB}(\bar{C}_\ell^{TE}\bar{C}_\ell^{TB} - \bar{C}_\ell^{TT}\bar{C}_\ell^{EB}) + \hat{C}_\ell^{BB}(\bar{C}_\ell^{TT}\bar{C}_\ell^{EE} - (\bar{C}_\ell^{TE})^2), \end{aligned} \quad (36)$$

$|\bar{C}|$ is the determinant of the theoretical covariance matrix [see Eq. (32)]:

$$|\bar{C}| = \bar{C}_\ell^{TT}\bar{C}_\ell^{EE}\bar{C}_\ell^{BB} + 2\bar{C}_\ell^{TE}\bar{C}_\ell^{TB}\bar{C}_\ell^{EB} - \bar{C}_\ell^{TT}(\bar{C}_\ell^{EB})^2 - \bar{C}_\ell^{EE}(\bar{C}_\ell^{TB})^2 - \bar{C}_\ell^{BB}(\bar{C}_\ell^{TE})^2, \quad (37)$$

and $|\hat{C}|$ is the determinant of the observed covariance matrix:

$$|\hat{C}| = \hat{C}_\ell^{TT}\hat{C}_\ell^{EE}\hat{C}_\ell^{BB} + 2\hat{C}_\ell^{TE}\hat{C}_\ell^{TB}\hat{C}_\ell^{EB} - \hat{C}_\ell^{TT}(\hat{C}_\ell^{EB})^2 - \hat{C}_\ell^{EE}(\hat{C}_\ell^{TB})^2 - \hat{C}_\ell^{BB}(\hat{C}_\ell^{TE})^2. \quad (38)$$

As a representative example for the next generation of CMB polarization experiments, we consider the Lite (Light) satellite for the study of B-mode polarization and inflation from cosmic background Lite background radiation detection (LiteBIRD) [85,86], selected by the Japan Aerospace Exploration Agency as a strategic large class mission. In Table I, we report the LiteBIRD-like experimental specifications that we use for our forecasts. We produce simulated data for T and E by considering the inverse noise weighting of the central frequency channels in Table I and by assuming that the lowest and highest frequencies are used to separate the foreground emission as done in Ref. [86] (see also Ref. [87]). For the B-mode polarization (in addition to the instrumental noise), we include the following two sources of confusion: the lensing signal and a contribution which mimics the foreground residuals, as also done in Ref. [88]. We compare these LiteBIRD-like noise power spectrum N_ℓ^{BB} with the signal induced by cosmic birefringence in Fig. 9. With these settings, we consider $f_{\mathrm{sky}} = 0.7$ and $\ell_{\mathrm{max}} = 1350$.

As a first step, we consider which constant birefringence angle $\bar{\alpha}$ could be detected with this LiteBIRD-like configuration. We consider a covariance matrix $\bar{C}$ obtained with $\bar{\alpha} = \{1, 0.5, 0.35, 0.2, 0.1, 0.01\}$ deg, and using the power spectra obtained from Eqs. (15)–(19) we estimated for some values of χ^2_{eff}; see Table II. The observed power spectra $\hat{C}_\ell$ correspond to the case without cosmic birefringence ($\alpha = 0$). We add, both to the theoretical and to the observed power spectra, the noise power spectra N_ℓ^{TT}, N_ℓ^{EE}, and N_ℓ^{BB} from Eq. (33); for C_ℓ^{BB}, we consider also the contribution of lensing and foregrounds.

TABLE I. Experimental specification for LiteBIRD: the full width half maximum ($\theta_{\mathrm{FWHM}\nu}$) and the detector noise levels for different frequency channels [85,89].

ν [GHz]	$\theta_{\mathrm{FWHM}\nu}$ [arcmin]	$\Delta_{T\nu}$ [μK arcmin]	$\Delta_{P\nu}$ [μK arcmin]
78	39	9.56	13.5
89	35	8.27	11.7
100	29	6.50	9.2
119	25	5.37	7.6
140	23	4.17	5.9
166	21	4.60	6.5
195	20	4.10	5.8

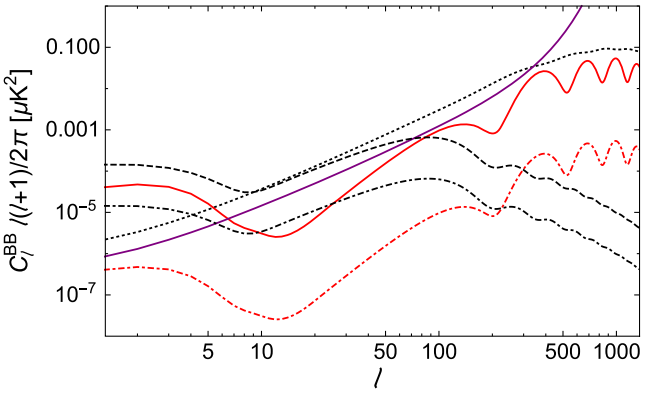

FIG. 9. Estimated noise power spectrum N_{lv}^{BB} for LiteBIRD (purple continuous line), compared with the signal induced by gravitational lensing (black dotted line), primordial signal for $r = 10^{-2}$ (black dashed line), primordial signal for $r = 10^{-3}$ (black dot-dashed line), signal induced by cosmic birefringence for $\bar{\alpha} = \pm 1$ deg (red continuous line), and signal induced by cosmic birefringence for $\bar{\alpha} = \pm 0.1$ deg (red dot-dashed line).

A. Limits for axionlike as early dark energy

We find that an axionlike field acting as EDE could produce a signal similar to the detection of $\bar{\alpha} = 0.35$ deg [48] by taking into account the redshift dependence of the scalar field with

$$g_\phi \sim 1.65 \times 10^{-18}\ \mathrm{GeV}^{-1}, \tag{39}$$

assuming, as in Sec. III A, $n = 2$, $\Lambda = 0.417$ eV, $f = 0.05 M_{\rm pl}$, $\Theta_i = 1$, and $\dot{\Theta}_i = 0$. We determine this value of g_ϕ by finding the C_ℓ obtained when taking into account the redshift dependence of the axionlike field acting as EDE which best mimics the $C_\ell^{\rm const}(\bar{\alpha} = 0.35\ \mathrm{deg})$ in Eqs. (15)–(19) by considering a minimization of $\Delta\chi^2_{\rm eff}$ in the presence of the lensing BB.

Let us now turn to future experiments such as LiteBIRD. It is important to note that a LiteBIRD-like experiment can, in principle, distinguish between the EDE signal induced by $g_\phi \sim 1.65 \times 10^{-18}$ GeV^{-1} and $C_\ell^{\rm const}(\bar{\alpha} = 0.35$ deg) at very high statistical significance, with $\chi^2_{\rm eff} = 67.3$ according to Table III. This capability of future experiments opens up the possibility to understand the physical mechanism of cosmological birefringence.

From Table III, we retrieve other important information. We report a value of $g_\phi \sim 1.4 \times 10^{-19}$ GeV^{-1} as the smallest value of the coupling which can be distinguished by a $C_\ell(\bar{\alpha})$ with $\bar{\alpha} = \alpha(\eta_{\rm rec}) - \alpha(\eta_0)$ in Eq. (14) and $g_\phi \sim 6.0 \times 10^{-20}$ GeV^{-1} as the 95% upper bound which a LiteBIRD-like experiment as the one we adopt can achieve.

Our results improve those obtained in Table I in Ref. [27] for LiteBIRD: $g_\phi \simeq 1.45 \times 10^{-16}$ GeV^{-1} (considering the power spectrum of the rotation angle $C_\ell^{\alpha\alpha}$) and $g_\phi \simeq 7.8 \times 10^{-17}$ GeV^{-1} (considering the cross-correlation between the rotation angle and the temperature $C_\ell^{\alpha T}$). See also the constraints for axionlike particles acting as early dark energy discussed in Ref. [31].

TABLE II. $\chi^2_{\rm eff}$ [see Eq. (35)] for different values of $\bar{\alpha}$: The theoretical power spectra are obtained using the analytic approximation of Eqs. (15)–(19), and they are compared to the unrotated case ($\alpha = 0$). We assume $f_{\rm sky} = 0.7$ and $\ell_{\rm max} = 1350$ for LiteBIRD.

$\bar{C}_\ell$ theoretical $(\bar{\alpha}) + N_\ell$	$\hat{C}_\ell$ observed $+ N_\ell$	$\chi^2_{\rm eff}$
$C_\ell(\bar{\alpha} = 1$ deg)	$C_\ell(\alpha = 0$ deg)	3.03×10^4
$C_\ell(\bar{\alpha} = 0.5$ deg)	$C_\ell(\alpha = 0$ deg)	7.57×10^3
$C_\ell(\bar{\alpha} = 0.35$ deg)	$C_\ell(\alpha = 0$ deg)	3.71×10^3
$C_\ell(\bar{\alpha} = 0.2$ deg)	$C_\ell(\alpha = 0$ deg)	1.12×10^3
$C_\ell(\bar{\alpha} = 0.1$ deg)	$C_\ell(\alpha = 0$ deg)	3.03×10^2
$C_\ell(\bar{\alpha} = 0.01$ deg)	$C_\ell(\alpha = 0$ deg)	3.03

TABLE III. Early dark energy: $\chi^2_{\rm eff}$ [see Eq. (35)] for different values of g_ϕ, at fixed $n = 2$, $\Lambda = 0.417$ eV, $f = 0.05 M_{\rm pl} = 1.22 \times 10^{17}$ GeV, $\Theta_i = 1$, and $\dot{\Theta}_i = 0$. The theoretical power spectra are obtained using the modified version of CAMB. The observed power spectra correspond to the case without cosmic birefringence ($\alpha = 0$), except the last two lines where we consider a rotation $\bar{\alpha}$; see Eqs. (15)–(19). We assume $f_{\rm sky} = 0.7$ and $\ell_{\rm max} = 1350$ for LiteBIRD.

$\bar{C}_\ell$ theoretical (EDE) $+ N_\ell$	$\hat{C}_\ell$ observed $+ N_\ell$	$\chi^2_{\rm eff}$
$C_\ell(g_\phi = 8.17 \times 10^{-18}\ \mathrm{GeV}^{-1})$	$C_\ell(\alpha = 0$ deg)	1.10×10^5
$C_\ell(g_\phi = 1.51 \times 10^{-18}\ \mathrm{GeV}^{-1})$	$C_\ell(\alpha = 0$ deg)	3.81×10^3
$C_\ell(g_\phi = 4.35 \times 10^{-19}\ \mathrm{GeV}^{-1})$	$C_\ell(\alpha = 0$ deg)	3.21×10^2
$C_\ell(g_\phi = 3.5 \times 10^{-19}\ \mathrm{GeV}^{-1})$	$C_\ell(\alpha = 0$ deg)	2.09×10^2
$C_\ell(g_\phi = 6.0 \times 10^{-20}\ \mathrm{GeV}^{-1})$	$C_\ell(\alpha = 0$ deg)	10.5
$C_\ell(g_\phi = 1.65 \times 10^{-18}\ \mathrm{GeV}^{-1})$	$C_\ell(\bar{\alpha} = 0.35$ deg)	67.3
$C_\ell(g_\phi = 1.4 \times 10^{-19}\ \mathrm{GeV}^{-1})$	$C_\ell(\bar{\alpha} = 0.02$ deg)	9.62

B. Limits for axionlike for dark energy

In the case of an axionlike field acting as dark energy, we find that we should consider a coupling constant of the order of

$$g_\phi \sim -1.8 \times 10^{-20}\ \mathrm{GeV}^{-1}, \tag{40}$$

in order to best mimic a birefringence signal $C_\ell^{\rm const}(\bar{\alpha} = 0.35$ deg) [48], assuming $M = 1.95 \times 10^{-3}$ eV, $f = 0.265 M_{\rm pl}$, $\Theta_i = 0.25$, and $\dot{\Theta}_i = 0$, as in Sec. III B. We always consider a minimization of $\Delta\chi^2_{\rm eff}$ in the presence of the lensing BB.

In this dark energy case, the pseudoscalar field ϕ becomes dynamic at late times, and, therefore, the linear polarization angle rotates at low redshift. The power spectra are quite similar to those obtained using the analytic

TABLE IV. Axionlike dark energy: $\chi^2_{\rm eff}$ [see Eq. (35)] for different values of g_ϕ, at fixed $M = 1.95\times10^{-3}$ eV, $f = 0.265 M_{\rm pl}$, $\Theta_i = 0.25$, and $\dot{\Theta}_i = 0$. The theoretical power spectra are obtained using the modified version of CAMB. The observed power spectra correspond to the case without cosmic birefringence ($\alpha = 0$), except the last two lines where we consider a rotation $\bar{\alpha}$; see Eqs. (15)–(19). We assume $f_{\rm sky} = 0.7$ and $\ell_{\rm max} = 1350$ for LiteBIRD.

$\bar{C}_\ell$ theoretical (DE) $+ N_\ell$	$\hat{C}_\ell$ observed $+ N_\ell$	$\chi^2_{\rm eff}$
$C_\ell(g_\phi = 1.8\times10^{-20}\ {\rm GeV}^{-1})$	$C_\ell(\alpha = 0\ {\rm deg})$	3.78×10^3
$C_\ell(g_\phi = 5.2\times10^{-21}\ {\rm GeV}^{-1})$	$C_\ell(\alpha = 0\ {\rm deg})$	3.15×10^2
$C_\ell(g_\phi = 7.2\times10^{-21}\ {\rm GeV}^{-1})$	$C_\ell(\alpha = 0\ {\rm deg})$	6.04×10^2
$C_\ell(g_\phi = 9.0\times10^{-22}\ {\rm GeV}^{-1})$	$C_\ell(\alpha = 0\ {\rm deg})$	9.4
$C_\ell(g_\phi = 8.0\times10^{-19}\ {\rm GeV}^{-1})$	$C_\ell(\bar{\alpha} = -15.7\ {\rm deg})$	9.8
$C_\ell(g_\phi = 1.8\times10^{-20}\ {\rm GeV}^{-1})$	$C_\ell(\bar{\alpha} = -0.35\ {\rm deg})$	0.30

TABLE V. Axionlike dark matter: $\chi^2_{\rm eff}$ [see Eq. (35)] for different values of g_ϕ, at fixed $m = 10^{-22}$ eV. The theoretical power spectra are obtained using the modified version of CAMB. The observed power spectra correspond to the case without cosmic birefringence ($\alpha = 0$), except the last two lines where we consider a rotation $\bar{\alpha}$; see Eqs. (15)–(19). We assume $f_{\rm sky} = 0.7$ and $\ell_{\rm max} = 1350$ for LiteBIRD.

$\bar{C}_\ell$ theoretical (DM) $+ N_\ell$	$\hat{C}_\ell$ observed $+ N_\ell$	$\chi^2_{\rm eff}$
$C_\ell(g_\phi = 1.5\times10^{-14}\ {\rm GeV}^{-1})$	$C_\ell(\alpha = 0\ {\rm deg})$	3.75×10^3
$C_\ell(g_\phi = 1.0\times10^{-14}\ {\rm GeV}^{-1})$	$C_\ell(\alpha = 0\ {\rm deg})$	1.70×10^4
$C_\ell(g_\phi = 4.3\times10^{-15}\ {\rm GeV}^{-1})$	$C_\ell(\alpha = 0\ {\rm deg})$	3.05×10^2
$C_\ell(g_\phi = 2.0\times10^{-15}\ {\rm GeV}^{-1})$	$C_\ell(\alpha = 0\ {\rm deg})$	66.0
$C_\ell(g_\phi = 8.1\times10^{-16}\ {\rm GeV}^{-1})$	$C_\ell(\alpha = 0\ {\rm deg})$	10.4
$C_\ell(g_\phi = 1.37\times10^{-14}\ {\rm GeV}^{-1})$	$C_\ell(\bar{\alpha} = 0.35\ {\rm deg})$	69.8
$C_\ell(g_\phi = 7.5\times10^{-15}\ {\rm GeV}^{-1})$	$C_\ell(\bar{\alpha} = 0.17\ {\rm deg})$	10.4

approximation in Eqs. (15)–(19). The smallest coupling g_ϕ that a LiteBIRD-like experiment can distinguish from $C_\ell^{\rm const}(\bar{\alpha})$ is $\sim 8.0\times10^{-19}$ GeV^{-1}, always assuming $\bar{\alpha} = \alpha(\eta_{\rm rec}) - \alpha(\eta_0)$. As 95% upper bound, we find $g_\phi \sim 9.0\times10^{-22}$ GeV^{-1} (see Table IV).

C. Limits for axionlike for dark matter

For a pseudoscalar field acting as dark matter, we find that

$$g_\phi \sim 1.37\times10^{-14}\ {\rm GeV}^{-1} \tag{41}$$

is needed to reproduce a signal similar to $\bar{\alpha} = 0.35$ deg [48] for $m = 10^{-22}$ eV, as in Sec. III C, by considering a minimization of $\Delta\chi^2_{\rm eff}$ in the presence of the lensing BB.

A LiteBIRD-like experiment can easily distinguish between a birefringence signal induced by dark matter with a coupling constant of this order of magnitude and $C_\ell^{\rm const}(\bar{\alpha} = 0.35\ {\rm deg})$ at very high statistical significance $\chi^2_{\rm eff} = 69.8$; see Table V.

From this table, we report also a value of $g_\phi \sim 7.5\times10^{-15}$ GeV^{-1} as the smallest value of the coupling which can be distinguished by a $C_\ell(\bar{\alpha})$ with $\bar{\alpha} = \alpha(\eta_{\rm rec}) - \alpha(\eta_0)$ in Eq. (14) and $g_\phi \sim 8.1\times10^{-16}$ GeV^{-1} as the 95% upper bound which a LiteBIRD-like experiment as the one we adopt can achieve.

The above results depend on the mass of the axion. If we consider a heavier mass for the pseudoscalar field, as $m = 10^{-20}$ eV, the coupling that mimics $C_\ell^{\rm const}(\bar{\alpha} = 0.35\ {\rm deg})$ is smaller than the one reported in Eq. (41) and is

$$g_\phi \sim 8.0\times10^{-13}\ {\rm GeV}^{-1}. \tag{42}$$

On the contrary, for smaller masses (e.g., $m = 10^{-20}$ eV), we have to consider a smaller coupling constant of the order of

$$g_\phi \sim 2.7\times10^{-16}\ {\rm GeV}^{-1}. \tag{43}$$

In Fig. 10, we compare the limits on the axion-photon coupling obtained from isotropic cosmic birefringence with the other limits present in the literature [90,91]. CMB cosmic birefringence nicely complements other experimental and astrophysical tests [92].

D. Markov chain Monte Carlo results

We perform few exploratory runs exploring the whole cosmological and birefringence parameter space using the MCMC code CosmoMC [93,94]. We use the exact Wishart likelihood with mock data generated following Eq. (35), with an effective sky fraction of 70% for all channels T, E, and B and including the same instrumental noise (see Fig. 9) and foreground residuals in BB. In order to include the full contribution of cosmic birefringence, we extended the standard exact likelihood to include also the odd cross-correlators TB and EB. We perform first an idealistic case where we vary only the coupling together with the six standard parameters of the ΛCDM: dark matter density $\Omega_c h^2$, baryon density $\Omega_{\rm B} h^2$, angular diameter distance to the last scattering surface θ, optical depth τ, the scalar spectral index n_s, and the amplitude of primordial fluctuations A_s. The resulting posterior probability distribution is shown in blue in Fig. 11, and the 68% error bar is $\sigma(g_\phi M_{\rm pl}/2) = 0.032$ with a fiducial $g_\phi = 0$ (corresponding to $|g_\phi| \lesssim 5.3\times10^{-20}$ GeV^{-1} at 2σ). Note that the degradation of a factor of few in the constraints in g_ϕ with respect to those quoted in Sec. IV is due to the variation of all the cosmological parameters in the MCMC exploration.

The result above mentioned represents an ideal case, because we have not included the uncertainty due to the miscalibration angle related to the uncertainty in the calibration of polarization angles. In order to account for such uncertainty, we add an isotropic rotation of the spectra

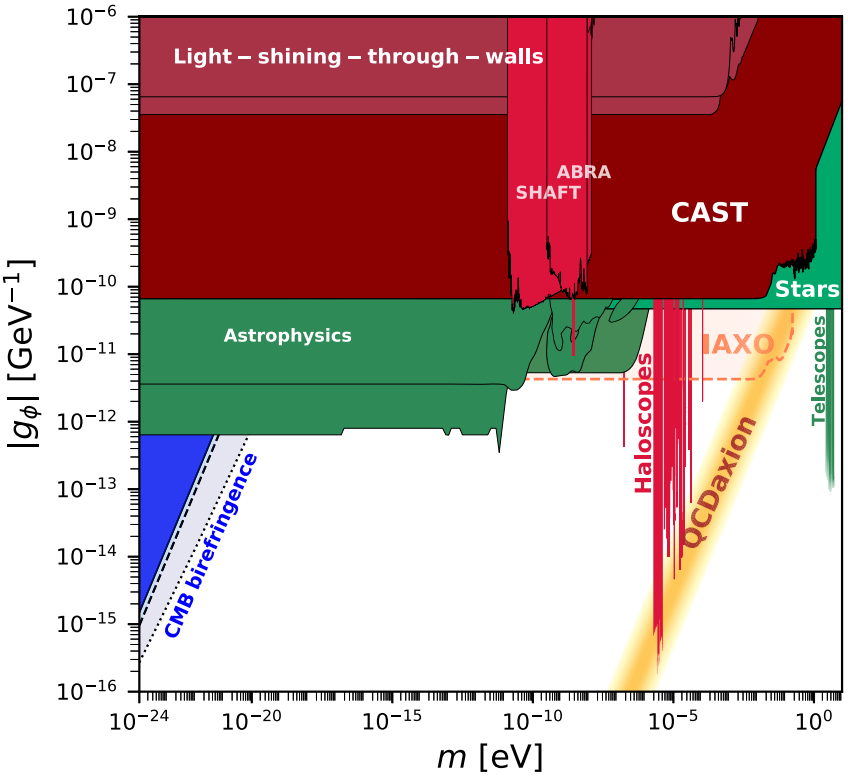

FIG. 10. Limits on the coupling constant with photons g_ϕ for a pseudoscalar field acting as dark matter as a function of mass m (colored regions are excluded). The light blue dotted line corresponds to CMB birefringence of the order of 0.35 deg [48] obtained by taking into account the redshift dependency of the birefringence angle, compared to CMB birefringence limits presented in Ref. [11] (dark blue region) and in Ref. [29] (blue dashed line). Plot created with the AxionLimits code [91]; we refer to online documentation for references on the other constraints.

due to an isotropic angle that we call $\alpha_{miscalib}$. This mimics the confusion created by not knowing the calibration angle when the birefringence signal arrives at the detectors. We vary this additional parameter assuming a Gaussian prior. We consider two cases: optimistic with a width of the prior of 0.00175 rad ($= 0.1$ deg $= 6$ arcmin) and pessimistic with a width of the prior of 0.0035 rad ($= 0.2$ deg $= 12$ arcmin). The resulting one-dimensional posteriors are presented in red and black in Fig. 11; we note how with respect to the blue ideal curve we have a slight degradation of the constraints on the coupling

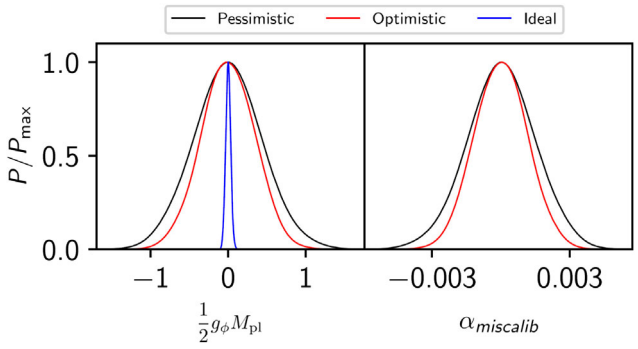

FIG. 11. One-dimensional posterior distribution for the coupling and the miscalibration angle. In blue, the ideal case where only the coupling is considered. In red, the optimistic case with the miscalibration angle, and in black, the pessimistic case.

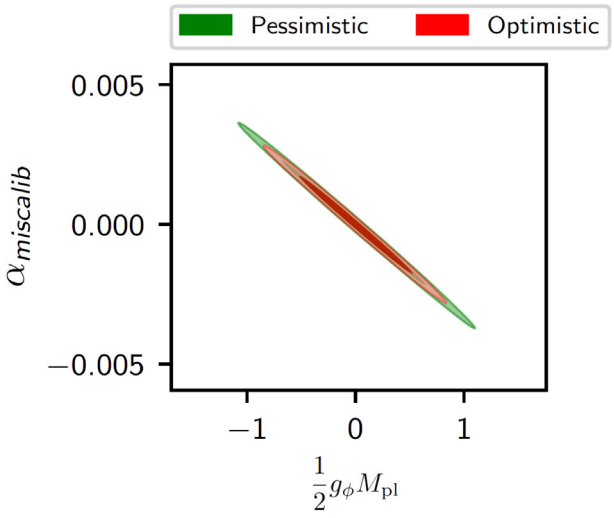

FIG. 12. Two-dimensional posterior distribution for the miscalibration angle vs the coupling. In green the pessimistic case, and in red the optimistic one.

whose uncertainty increase by roughly one order of magnitude to $\sigma(g_\phi M_{\rm pl}/2) = 0.35$ (corresponding to $|g_\phi| \lesssim 5.7 \times 10^{-19}$ GeV^{-1} at 2σ) for the optimistic and $\sigma(g_\phi M_{\rm pl}/2) = 0.41$ (corresponding to $|g_\phi| \lesssim 6.7 \times 10^{-19}$ GeV^{-1} at 2σ) for the pessimistic case. Note that the constraints on g_ϕ obtained by taking into account the miscalibration angle degrade by roughly one order of magnitude.

In Fig. 12, we show the correlation between the miscalibration angle and the coupling. Note that the degeneracy in the miscalibration angle and the coupling is not exact as would be with the birefringence angle when the redshift dependence of the rotation angle is neglected.

V. CONCLUSIONS

We studied isotropic cosmological birefringence induced by a cosmological redshift-dependent pseudoscalar field with a coupling $g_\phi \phi F^{\mu\nu}\tilde{F}_{\mu\nu}$. We showed how time evolution of the background pseudoscalar field imprints, in general, a nontrivial multipole dependence in the observed CMB angular power spectra which is not captured by the widely adopted approximation in which the redshift dependence of the rotation angle is neglected. This effect could be important in interpreting reported hints of birefringence in the Planck CMB spectra [48,49,51,52]. Beyond considering phenomenological redshift evolution for the rotation angle induced by a pseudoscalar field, we also considered the theoretical prediction for early dark energy, quintessence, and axionlike matter.

As consequences, not only the total rotation $\bar{\alpha} = \alpha(\eta_{\rm rec}) - \alpha(\eta_0)$ determines the final CMB spectra, but also when the rotation occurs compared to the main changes in the visibility function, i.e., recombination and reionization. Moreover, nonvanishing parity-violating effects occur also in the particular case $\alpha(\eta_{\rm rec}) = \alpha(\eta_0)$.

Because of the nontrivial multipole dependence induced by the redshift evolution of the pseudoscalar field, the resulting isotropic birefringence is not degenerate with a polarization rotation angle independent on the multipoles, which is connected to a systematic calibration angle uncertainty.

For the theoretical models of EDE, DE, and axionlike DM, we estimated the size of the couplings which will be detected by a LiteBIRD-like experiment by a χ^2 calculation. Moreover, always for these models and by a χ^2 calculation, we also computed at which level our theoretical predictions can be distinguished by the widely adopted approximation in which the redshift dependence of the rotation angle is neglected for a LiteBIRD-like experiment. Finally, we have explicitly shown by MCMC the reduction of the degeneracy between the isotropic birefringence effect for early dark energy and the miscalibration angle by allowing all the cosmological parameters to vary, always for a LiteBIRD-like experiment.

As a next step, we will add the effects due inhomogeneities in the pseudoscalar field, i.e., anisotropic birefringence, to complete the theoretical predictions of interesting models with a pseudoscalar field, such as early dark energy, quintessence, and axionlike matter.

ACKNOWLEDGMENTS

We thank A. Gruppuso and E. Komatsu for useful discussions. F. F. and D. P. acknowledge financial support by ASI Grant No. 2016-24-H.0 and Agreement No. 2020-9-HH.0 ASI-UniRM2. We acknowledge the use of the Istituto Nazionale di Astrofisica - Osservatorio di Astrofisica e Scienza dello Spazio Bologna (INAF-OAS) High Performance Computing (HPC) cluster.

APPENDIX: ADDITIONAL PHENOMENOLOGICAL POWER SPECTRA

In this appendix, we discuss other phenomenological examples of redshift dependence of the linear polarization angle.

First, we consider "instantaneous rotation at present time" (see Fig. 13). In this case, $\bar{\alpha} = \alpha(\eta_{\rm rec}) - \alpha(\eta_0)$ is exactly constant during integration along the line of sight; therefore, the power spectra obtained using the modified CAMB code (colored lines) exactly coincide with the $C_\ell^{\rm obs}$ given by the analytic expressions in Eqs. (15)–(19) (colored regions).

The comparison between Figs. 2 and 14 assures us that the effects on the power spectra are not dominated by the slope of the tanh function describing the transition between two different values of the linear polarization angle. Instead, it is very important when this transition occurs: The earlier in time the rotation happens, the smaller are the effects on the power spectra.

In Fig. 4, we already showed that power spectra are influenced by cosmic birefringence also when $\bar{\alpha} = \alpha(\eta_{\rm rec}) - \alpha(\eta_0) = 0$. In Fig. 15, we always focus on an oscillating behavior with $\bar{\alpha} = 0$, but we compare different frequencies. Effects on the power spectra at high ℓ seem to increase at higher oscillating frequencies [$\alpha(\eta) = \sin(10\pi x)$ and $\alpha(\eta) = \sin(100\pi x)$], but for a linear polarization angle oscillating extremely quickly [e.g., $\alpha(\eta) = \sin(1000\pi x)$] the effects cancel out. Since the visibility function reaches its maximum at recombination and a second peak at reionization—see Sec. II for more details—the overall effects highly depend on the value of $\alpha(\eta) - \alpha(\eta_0)$ at these two epochs. In the case $\alpha(\eta) = \sin(\pi x)$, the birefringence angle is too small at recombination to modify the source terms in Eqs. (11) and (12), but effects are visible at reionization (lower ℓ). On the contrary, for $\alpha(\eta) = \sin(10\pi x)$ and $\alpha(\eta) = \sin(100\pi x)$, the effects at recombination (high ℓ) are quite important, while the effects at low ℓ (reionization) are wiped out by the rapid oscillations of the birefringence angle; for even faster

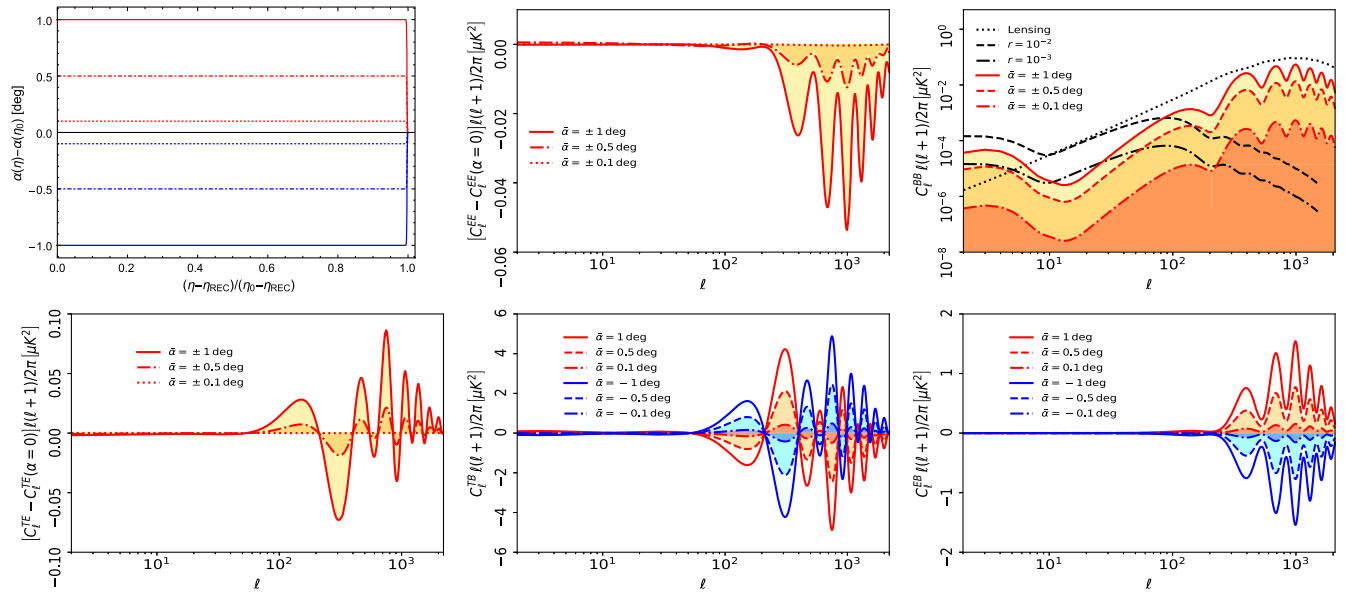

FIG. 13. (a) Evolution of $\alpha(\eta) - \alpha(\eta_0)$ as a function of conformal time: during propagation $\bar{\alpha} = \pm 1$ deg (continue red and blue lines), ± 0.5 deg (dashed red and blue lines), and ± 0.1 deg (dotted red and blue lines). In this case, the output of the modified CAMB code (colored lines) coincides with the analytic approximations in Eqs. (15)–(19) (colored regions): (b) $C_\ell^{EE} - C_\ell^{EE}(\bar{\alpha} = 0)$, (c) C_ℓ^{BB}, (d) $C_\ell^{TE} - C_\ell^{TE}(\bar{\alpha} = 0)$, (e) C_ℓ^{TB}, and (f) C_ℓ^{EB}.

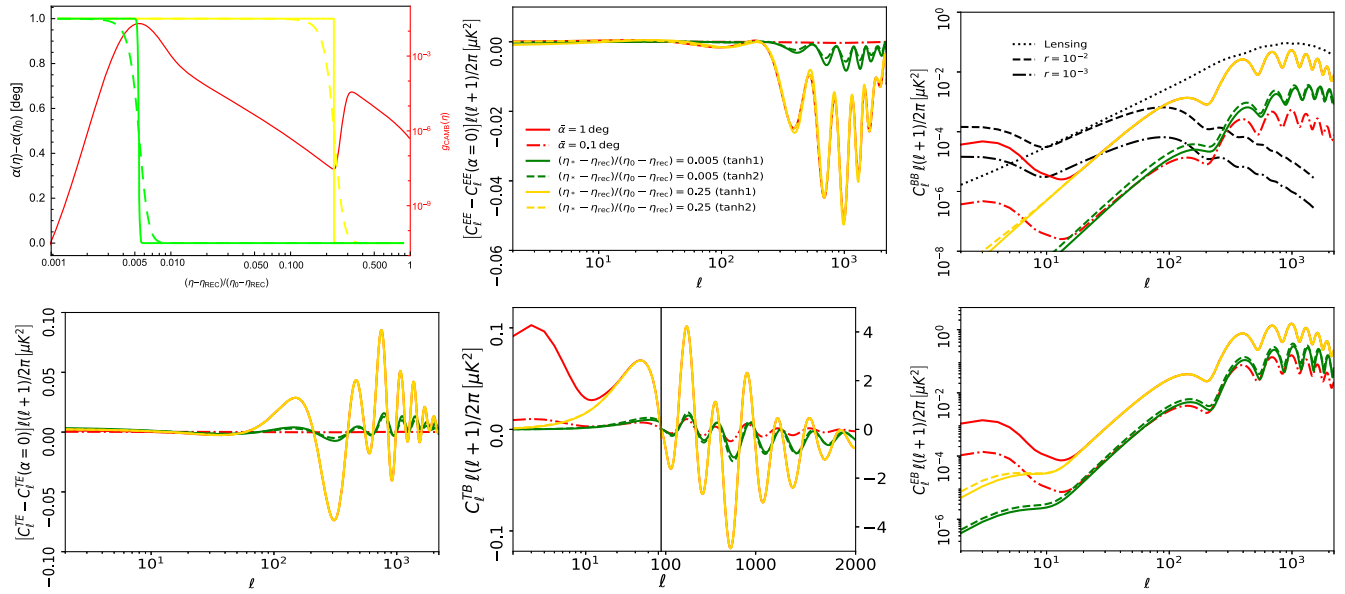

FIG. 14. Comparison between different hyperbolic tangents: (a) evolution of $\alpha(\eta) - \alpha(\eta_0)$ as a function of conformal time $x \equiv (\eta - \eta_{\rm rec})/(\eta_0 - \eta_{\rm rec})$: $\alpha(\eta) = -1/2\{1 + \tanh[10^4(x - 0.005)]\}$ (green continuous line), $\alpha(\eta) = -1/2\{1 + \tanh[10^3(x - 0.005)]\}$ (green dotted line), $\alpha(\eta) = -1/2\{1 + \tanh[10^4(x - 0.25)]\}$ (yellow dotted line), $\alpha(\eta) = -1/2\{1 + \tanh[20(x - 0.25)]\}$ (yellow dotted line)—the CAMB visibility function $g_{\rm CAMB}$ is plotted in red (on a different scale); angular power spectra obtained with the modified version of CAMB are compared in (b) $C_\ell^{EE} - C_\ell^{EE}(\bar{\alpha} = 0)$, (c) C_ℓ^{BB}, (d) $C_\ell^{TE} - C_\ell^{TE}(\bar{\alpha} = 0)$, (e) C_ℓ^{TB}, and (f) C_ℓ^{EB}.

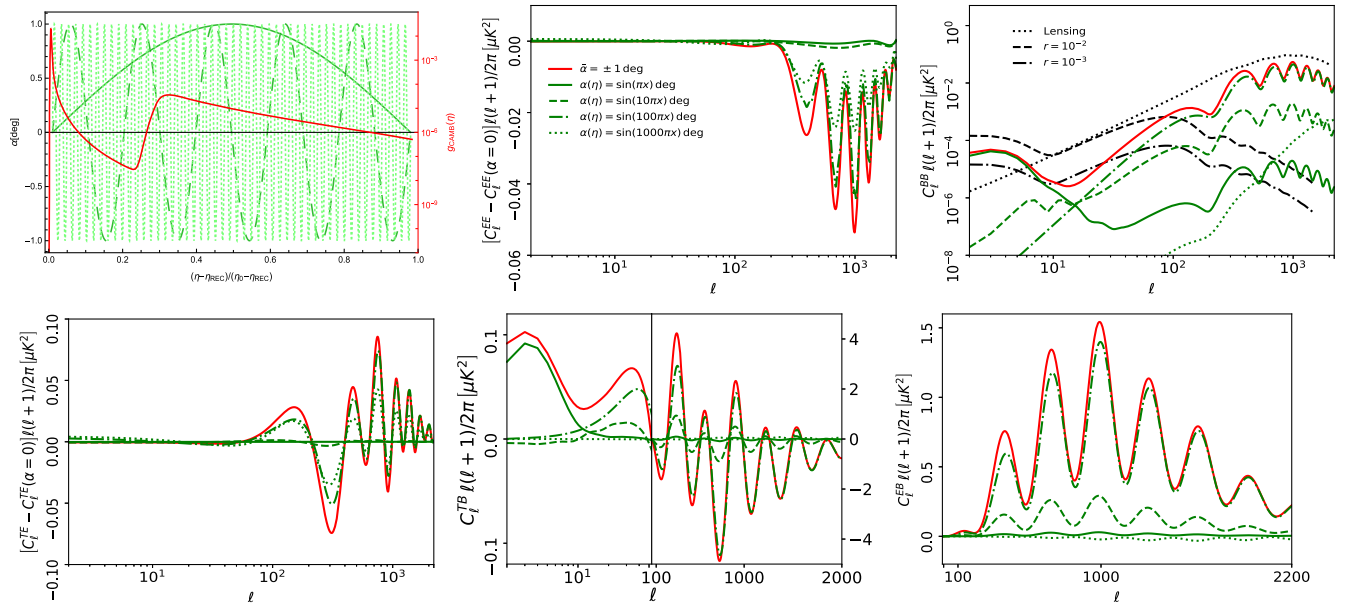

FIG. 15. (a) Evolution of the birefringence angle α as a function of conformal time $x \equiv (\eta - \eta_{\rm rec})/(\eta_0 - \eta_{\rm rec})$: $\alpha(\eta) = \sin(\pi x)$ (green continuous line), $\alpha(\eta) = \sin(10\pi x)$ (green dotted line), $\alpha(\eta) = \sin(100\pi x)$ (green dot-dashed line), and $\alpha(\eta) = \sin(1000\pi x)$ (green dotted line)—note that in all three cases $\alpha(\eta_{\rm rec}) = \alpha(\eta_0)$ ($\bar{\alpha} = 0$ deg)—the CAMB visibility function $g_{\rm CAMB}$ is plotted in red (on a different scale); (b) $C_\ell^{EE} - C_\ell^{EE}(\bar{\alpha} = 0)$, (c) C_ℓ^{BB}, (d) $C_\ell^{TE} - C_\ell^{TE}(\bar{\alpha} = 0)$, (e) C_ℓ^{TB}, and (f) C_ℓ^{EB}.

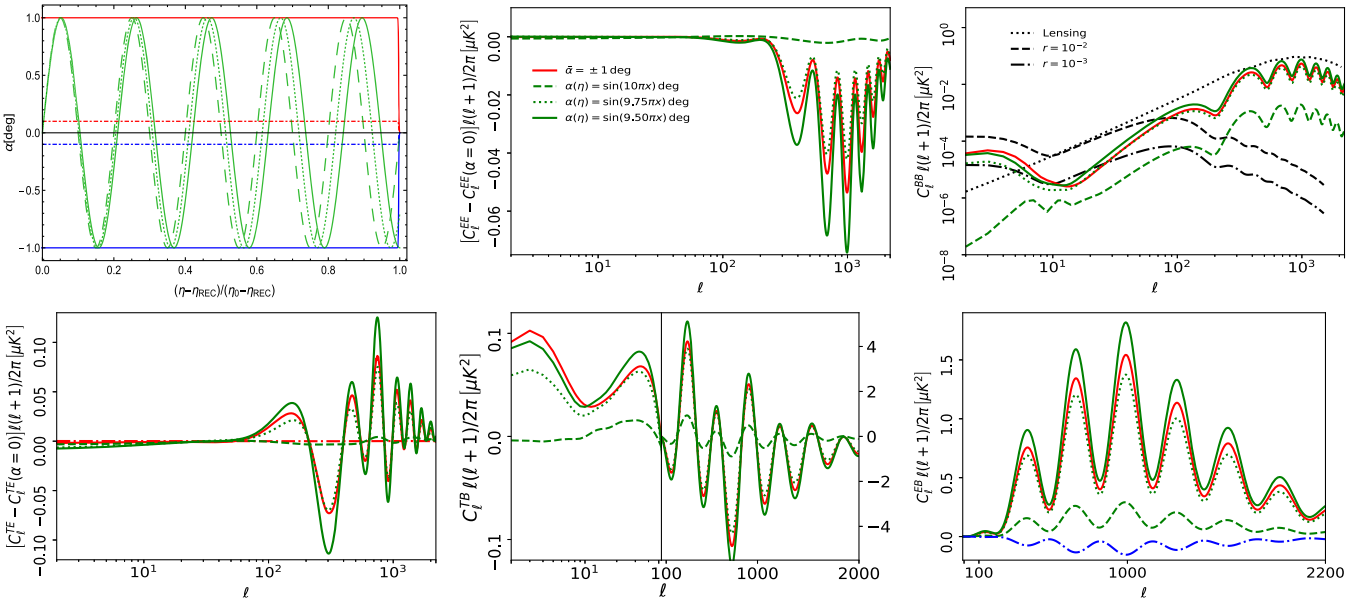

FIG. 16. (a) Evolution of the birefringence angle α as a function of conformal time $x \equiv (\eta - \eta_{\rm rec})/(\eta_0 - \eta_{\rm rec})$: $\alpha(\eta) = \sin(9.5\pi x)$ (green continuous line, $\bar{\alpha} = 1$ deg), $\alpha(\eta) = \sin(9.75\pi x)$ (green dotted line, $\bar{\alpha} = 0.71$ deg), and $\alpha(\eta) = \sin(10\pi x)$ (green dashed line, $\bar{\alpha} = 0$ deg)—we plot for comparison also the case of a sudden rotation of ± 1 deg (± 0.1 deg) occurring at the present time; see the continuous (dot-dashed) red and blue lines. (b) $C_\ell^{EE} - C_\ell^{EE}(\bar{\alpha} = 0)$, (c) C_ℓ^{BB}, (d) $C_\ell^{TE} - C_\ell^{TE}(\bar{\alpha} = 0)$, (e) C_ℓ^{TB}, and (f) C_ℓ^{EB}.

oscillations, $\alpha(\eta) = \sin(1000\pi x)$, the effects are deleted also at recombination.

Finally (see Fig. 16), we compare three different oscillating behaviors of the linear polarization angle. In one case $\alpha(\eta_{\rm rec}) = \alpha(\eta_0)$, while in the other two cases $\alpha(\eta_{\rm rec}) \neq \alpha(\eta_0)$. When there is a difference between the value of α at recombination and today, this clearly dominates the effects on the power spectra.

[1] S. M. Carroll, G. B. Field, and R. Jackiw, Limits on a Lorentz and parity violating modification of electrodynamics, Phys. Rev. D **41**, 1231 (1990).

[2] D. Harari and P. Sikivie, Effects of a Nambu-Goldstone boson on the polarization of radio galaxies and the cosmic microwave background, Phys. Lett. B **289**, 67 (1992).

[3] S. M. Carroll and G. B. Field, The Einstein equivalence principle and the polarization of radio galaxies, Phys. Rev. D **43**, 3789 (1991).

[4] A. Cimatti, S. di Serego Alighieri, G. B. Field, and R. A. E. Fosbury, Stellar and scattered light in a radio galaxy at $z = 2.63$, Astrophys. J. **422**, 562 (1994).

[5] S. M. Carroll and G. B. Field, Is There Evidence for Cosmic Anisotropy in the Polarization of Distant Radio Sources?, Phys. Rev. Lett. **79**, 2394 (1997).

[6] S. M. Carroll, Quintessence and the Rest of the World, Phys. Rev. Lett. **81**, 3067 (1998).

[7] S. di Serego Alighieri, F. Finelli, and M. Galaverni, Limits on cosmological birefringence from the UV polarization of distant radio galaxies, Astrophys. J. **715**, 33 (2010).

[8] A. Lue, L. M. Wang, and M. Kamionkowski, Cosmological Signature of New Parity Violating Interactions, Phys. Rev. Lett. **83**, 1506 (1999).

[9] B. Feng, H. Li, M. z. Li, and X. m. Zhang, Gravitational leptogenesis and its signatures in CMB, Phys. Lett. B **620**, 27 (2005).

[10] B. Feng, M. Li, J. Q. Xia, X. Chen, and X. Zhang, Searching for *CPT* Violation with Cosmic Microwave Background Data from WMAP and BOOMERANG, Phys. Rev. Lett. **96**, 221302 (2006).

[11] F. Finelli and M. Galaverni, Rotation of linear polarization plane and circular polarization from cosmological pseudoscalar fields, Phys. Rev. D **79**, 063002 (2009).

[12] S. Alexander, J. Ochoa, and A. Kosowsky, Generation of circular polarization of the cosmic microwave background, Phys. Rev. D **79**, 063524 (2009).

[13] G. C. Liu, S. Lee, and K. W. Ng, Effect on Cosmic Microwave Background Polarization of Coupling of Quintessence to Pseudoscalar Formed from the Electromagnetic Field and its Dual, Phys. Rev. Lett. **97**, 161303 (2006).

[14] G. Gubitosi, M. Martinelli, and L. Pagano, Including birefringence into time evolution of CMB: Current and future constraints, J. Cosmol. Astropart. Phys. 12 (2014) 020.

[15] S. Chigusa, T. Moroi, and K. Nakayama, Signals of axion like dark matter in time dependent polarization of light, Phys. Lett. B **803**, 135288 (2020).

[16] B. D. Sherwin and T. Namikawa, Cosmic birefringence tomography and calibration-independence with reionization signals in the CMB, arXiv:2108.09287.

[17] H. Nakatsuka, T. Namikawa, and E. Komatsu, Is cosmic birefringence due to dark energy or dark matter? A tomographic approach, Phys. Rev. D **105**, 123509 (2022).

[18] A. Greco, N. Bartolo, and A. Gruppuso, Probing axions through tomography of anisotropic cosmic birefringence, arXiv:2211.06380.

[19] M. Li and X. Zhang, Cosmological *CPT* violating effect on CMB polarization, Phys. Rev. D **78**, 103516 (2008).

[20] M. Pospelov, A. Ritz, and C. Skordis, Pseudoscalar Perturbations and Polarization of the Cosmic Microwave Background, Phys. Rev. Lett. **103**, 051302 (2009).

[21] M. Kamionkowski, How to De-Rotate the Cosmic Microwave Background Polarization, Phys. Rev. Lett. **102**, 111302 (2009).

[22] H. Cai and Y. Guan, Computing microwave background polarization power spectra from cosmic birefringence, Phys. Rev. D **105**, 063536 (2022).

[23] A. Greco, N. Bartolo, and A. Gruppuso, Cosmic birefrigence: Cross-spectra and cross-bispectra with CMB anisotropies, J. Cosmol. Astropart. Phys. 03 (2022) 050.

[24] G. Gubitosi, L. Pagano, G. Amelino-Camelia, A. Melchiorri, and A. Cooray, A Constraint on planck-scale modifications to electrodynamics with CMB polarization data, J. Cosmol. Astropart. Phys. 08 (2009) 021.

[25] G. C. Liu and K. W. Ng, Axion dark matter induced cosmic microwave background *B*-modes, Phys. Dark Universe **16**, 22 (2017).

[26] G. Sigl and P. Trivedi, Axionlike dark matter constraints from CMB birefringence, arXiv:1811.07873.

[27] L. M. Capparelli, R. R. Caldwell, and A. Melchiorri, Cosmic birefringence test of the Hubble tension, Phys. Rev. D **101**, 123529 (2020).

[28] T. Fujita, Y. Minami, K. Murai, and H. Nakatsuka, Probing axionlike particles via cosmic microwave background polarization, Phys. Rev. D **103**, 063508 (2021).

[29] M. A. Fedderke, P. W. Graham, and S. Rajendran, Axion dark matter detection with CMB polarization, Phys. Rev. D **100**, 015040 (2019).

[30] K. Murai, F. Naokawa, T. Namikawa, and E. Komatsu, Isotropic cosmic birefringence from early dark energy, Phys. Rev. D **107**, L041302 (2023).

[31] T. Fujita, K. Murai, H. Nakatsuka, and S. Tsujikawa, Detection of isotropic cosmic birefringence and its implications for axionlike particles including dark energy, Phys. Rev. D **103**, 043509 (2021).

[32] E. Komatsu *et al.* (WMAP Collaboration), Seven-year Wilkinson Microwave Anisotropy Probe (WMAP) observations: Cosmological interpretation, Astrophys. J. Suppl. Ser. **192**, 18 (2011).

[33] A. Gruppuso, P. Natoli, N. Mandolesi, A. De Rosa, F. Finelli, and F. Paci, WMAP 7 year constraints on *CPT* violation from large angle CMB anisotropies, J. Cosmol. Astropart. Phys. 02 (2012) 023.

[34] F. Finelli, A. De Rosa, A. Gruppuso, and D. Paoletti, Cosmological Parameters from a re-analysis of the WMAP-7 low resolution maps, Mon. Not. R. Astron. Soc. **431**, 2961 (2013).

[35] A. Gruppuso, M. Gerbino, P. Natoli, L. Pagano, N. Mandolesi, A. Melchiorri, and D. Molinari, Constraints on cosmological birefringence from Planck and Bicep2/Keck data, J. Cosmol. Astropart. Phys. 06 (2016) 001.

[36] N. Aghanim *et al.* (Planck Collaboration), Planck intermediate results. XLIX. Parity-violation constraints from polarization data, Astron. Astrophys. **596**, A110 (2016).

[37] P. A. R. Ade *et al.* (POLARBEAR Collaboration), A measurement of the cosmic microwave background *B*-mode polarization power spectrum at sub-degree scales from 2 years of POLARBEAR data, Astrophys. J. **848**, 121 (2017).

[38] W. L. K. Wu, L. M. Mocanu, P. A. R. Ade, A. J. Anderson, J. E. Austermann, J. S. Avva, J. A. Beall, A. N. Bender, B. A. Benson, F. Bianchini *et al.*, A measurement of the

cosmic microwave background lensing potential and power spectrum from 500 deg^2 of SPTpol temperature and polarization data, Astrophys. J. **884**, 70 (2019).
[39] A. Gruppuso, D. Molinari, P. Natoli, and L. Pagano, Planck 2018 constraints on anisotropic birefringence and its cross-correlation with CMB anisotropy, J. Cosmol. Astropart. Phys. 11 (2020) 066.
[40] P. A. R. Ade *et al.* (BICEP/Keck Collaboration), BICEP/Keck XII: Constraints on axionlike polarization oscillations in the cosmic microwave background, Phys. Rev. D **103**, 042002 (2021).
[41] P. A. R. Ade *et al.* (BICEP/Keck Collaboration), BICEP/Keck XIV: Improved constraints on axionlike polarization oscillations in the cosmic microwave background, Phys. Rev. D **105**, 022006 (2022).
[42] T. Namikawa, Y. Guan, O. Darwish, B. D. Sherwin, S. Aiola, N. Battaglia, J. A. Beall, D. T. Becker, J. R. Bond, E. Calabrese *et al.*, Atacama cosmology telescope: Constraints on cosmic birefringence, Phys. Rev. D **101**, 083527 (2020).
[43] M. Bortolami, M. Billi, A. Gruppuso, P. Natoli, and L. Pagano, Planck constraints on cross-correlations between anisotropic cosmic birefringence and CMB polarization, J. Cosmol. Astropart. Phys. 09 (2022) 075.
[44] K. N. Abazajian *et al.* (CMB-S4 Collaboration), CMB-S4 science book, first edition, arXiv:1610.02743.
[45] D. Molinari, A. Gruppuso, and P. Natoli, Constraints on parity violation from ACTpol and forecasts for forthcoming CMB experiments, Phys. Dark Universe **14**, 65 (2016).
[46] S. Hanany *et al.* (NASA PICO Collaboration), PICO: Probe of inflation and cosmic origins, arXiv:1902.10541.
[47] L. Pogosian, M. Shimon, M. Mewes, and B. Keating, Future CMB constraints on cosmic birefringence and implications for fundamental physics, Phys. Rev. D **100**, 023507 (2019).
[48] Y. Minami and E. Komatsu, New Extraction of the Cosmic Birefringence from the Planck 2018 Polarization Data, Phys. Rev. Lett. **125**, 221301 (2020).
[49] P. Diego-Palazuelos, J. R. Eskilt, Y. Minami, M. Tristram, R. M. Sullivan, A. J. Banday, R. B. Barreiro, H. K. Eriksen, K. M. Górski, R. Keskitalo *et al.*, Cosmic Birefringence from the Planck Data Release 4, Phys. Rev. Lett. **128**, 091302 (2022).
[50] Y. Akrami *et al.* (Planck Collaboration), Planck intermediate results. LVII. Joint Planck LFI and HFI data processing, Astron. Astrophys. **643**, A42 (2020).
[51] J. R. Eskilt and E. Komatsu, Improved constraints on cosmic birefringence from the WMAP and Planck cosmic microwave background polarization data, Phys. Rev. D **106**, 063503 (2022).
[52] E. Komatsu, New physics from polarised light of the cosmic microwave background, Nat. Rev. Phys. **4**, 452 (2022).
[53] N. Aghanim *et al.* (Planck Collaboration), Planck 2018 results. VI. Cosmological parameters, Astron. Astrophys. **641**, A6 (2020); **652**, C4(E) (2021).
[54] M. Galaverni, G. Gubitosi, F. Paci, and F. Finelli, Cosmological birefringence constraints from CMB and astrophysical polarization data, J. Cosmol. Astropart. Phys. 08 (2015) 031.
[55] M. Galaverni, Testing new physics with polarized light: Cosmological birefringence, Astrophys. Space Sci. Proc. **51**, 165 (2018).
[56] S. di Serego Alighieri, The conventions for the polarization angle, Exper. Astron. **43**, 19 (2017).
[57] A. Kosowsky and A. Loeb, Faraday rotation of microwave background polarization by a primordial magnetic field, Astrophys. J. **469**, 1 (1996).
[58] U. Seljak and M. Zaldarriaga, A line of sight integration approach to cosmic microwave background anisotropies, Astrophys. J. **469**, 437 (1996).
[59] A. Lewis, A. Challinor, and A. Lasenby, Efficient computation of CMB anisotropies in closed FRW models, Astrophys. J. **538**, 473 (2000).
[60] A. Gruppuso, G. Maggio, D. Molinari, and P. Natoli, A note on the birefringence angle estimation in CMB data analysis, J. Cosmol. Astropart. Phys. 05 (2016) 020.
[61] Y. Minami, H. Ochi, K. Ichiki, N. Katayama, E. Komatsu, and T. Matsumura, Simultaneous determination of the cosmic birefringence and miscalibrated polarization angles from CMB experiments, Prog. Theor. Exp. Phys. **2019**, 083E02 (2019).
[62] B. G. Keating, M. Shimon, and A. P. S. Yadav, Self-calibration of cosmic microwave background polarization experiments, Astrophys. J. Lett. **762**, L23 (2013).
[63] Y. Minami and E. Komatsu, Simultaneous determination of the cosmic birefringence and miscalibrated polarization angles II: Including cross frequency spectra, Prog. Theor. Exp. Phys. **2020**, 103E02 (2020).
[64] T. Namikawa, CMB mode coupling with isotropic polarization rotation, Mon. Not. R. Astron. Soc. **506**, 1250 (2021).
[65] V. Poulin, T. L. Smith, D. Grin, T. Karwal, and M. Kamionkowski, Cosmological implications of ultralight axionlike fields, Phys. Rev. D **98**, 083525 (2018).
[66] V. Poulin, T. L. Smith, T. Karwal, and M. Kamionkowski, Early Dark Energy Can Resolve The Hubble Tension, Phys. Rev. Lett. **122**, 221301 (2019).
[67] P. B. Greene, L. Kofman, A. D. Linde, and A. A. Starobinsky, Structure of resonance in preheating after inflation, Phys. Rev. D **56**, 6175 (1997).
[68] F. Finelli and R. H. Brandenberger, Parametric Amplification of Gravitational Fluctuations During Reheating, Phys. Rev. Lett. **82**, 1362 (1999).
[69] M. Abramowitz and I. A. Stegun, *Handbook of Mathematical Functions with Formulas, Graphs, and Mathematical Tables* (Dover, New York, 1964).
[70] In order to insert the elliptic sine $\mathrm{sn}(x, \frac{1}{\sqrt{2}})$ in the CAMB code, we applied a twice descending Landen transformation (see Sec. 16.12 in Ref. [69]):

$$\mathrm{sn}(x,m) = \frac{\left(1+\mu_1^{1/2}\right)\mathrm{sn}\left(\frac{x}{1+\mu_1^{1/2}},\mu_1\right)}{1+\mu_1^{1/2}\mathrm{sn}^2\left(\frac{x}{1+\mu_1^{1/2}},\mu_1\right)},$$

where

$$\mu_1 \equiv \left(\frac{1-\sqrt{1-m}}{1+\sqrt{1-m}}\right)^2.$$

Starting from $m = 1/\sqrt{2} \simeq 0.707$, we obtained first $\mu_1 \simeq 0.089$, and applying the Landen transformation a second time $\mu_2 \simeq 0.00053$. Finally, since we reduced to a

case where $m \ll 1$, we used the approximation of the elliptic sine in terms of circular functions (see Sec. 16.12 in Ref. [69]):

$$\mathrm{sn}(x, m) \simeq \sin x - \frac{m}{4}(x - \sin x \cos x)\cos x.$$

[71] T. L. Smith, V. Poulin, and M. A. Amin, Oscillating scalar fields and the Hubble tension: a resolution with novel signatures, Phys. Rev. D **101**, 063523 (2020).

[72] J. A. Frieman, C. T. Hill, A. Stebbins, and I. Waga, Cosmology with Ultralight Pseudo Nambu-Goldstone Bosons, Phys. Rev. Lett. **75**, 2077 (1995).

[73] M. Dine, Dark matter and dark energy: A physicist's perspective, arXiv:hep-th/0107259.

[74] T. Banks, M. Dine, P. J. Fox, and E. Gorbatov, On the possibility of large axion decay constants, J. Cosmol. Astropart. Phys. 06 (2003) 001.

[75] P. Sikivie, Experimental Tests of the Invisible Axion, Phys. Rev. Lett. **51**, 1415 (1983); **52**, 695(E) (1984).

[76] G. G. Raffelt, *Stars as Laboratories for Fundamental Physics: The Astrophysics of Neutrinos, Axions, and Other Weakly Interacting Particles* (Chicago University Press, Chicago, 1996).

[77] E. W. Kolb and M. S. Turner, The early universe, Front. Phys. **69**, 1 (1990).

[78] P. Sikivie, Axion cosmology, Lect. Notes Phys. **741**, 19 (2008).

[79] M. Galaverni and F. Finelli, Rotation of linear polarization plane from cosmological pseudoscalar fields, Nucl. Phys. B, Proc. Suppl. **194**, 51 (2009).

[80] A. Gruppuso and F. Finelli, Analytic results for a flat universe dominated by dust and dark energy, Phys. Rev. D **73**, 023512 (2006).

[81] F. Finelli *et al.* (CORE Collaboration), Exploring cosmic origins with CORE: Inflation, J. Cosmol. Astropart. Phys. 04 (2018) 016.

[82] R. Easther, W. H. Kinney, and H. Peiris, Observing trans-Planckian signatures in the cosmic microwave background, J. Cosmol. Astropart. Phys. 05 (2005) 009.

[83] J. Q. Xia, H. Li, G. B. Zhao, and X. Zhang, Probing for the cosmological parameters with PLANCK measurement, Int. J. Mod. Phys. D **17**, 2025 (2009).

[84] J. Q. Xia, H. Li, X. l. Wang, and X. m. Zhang, Testing *CPT* symmetry with CMB measurements, Astron. Astrophys. **483**, 715 (2008).

[85] M. Hazumi, P. A. R. Ade, Y. Akiba, D. Alonso, K. Arnold, J. Aumont, C. Baccigalupi, D. Barron, S. Basak, S. Beckman *et al.*, LiteBIRD: A satellite for the studies of B-mode polarization and inflation from cosmic background radiation detection, J. Low Temp. Phys. **194**, 443 (2019).

[86] E. Allys *et al.* (LiteBIRD Collaboration), Probing cosmic inflation with the LiteBIRD cosmic microwave background polarization survey, arXiv:2202.02773.

[87] F. Finelli *et al.* (CORE Collaboration), Exploring cosmic origins with CORE: Inflation, J. Cosmol. Astropart. Phys. 04 (2018) 016.

[88] D. Paoletti, F. Finelli, J. Valiviita, and M. Hazumi, Planck and BICEP/Keck Array 2018 constraints on primordial gravitational waves and perspectives for future B-mode polarization measurements, Phys. Rev. D **106**, 083528 (2022).

[89] D. Paoletti and F. Finelli, Constraints on primordial magnetic fields from magnetically-induced perturbations: Current status and future perspectives with LiteBIRD and future ground based experiments, J. Cosmol. Astropart. Phys. 11 (2019) 028.

[90] R. L. Workman *et al.* (Particle Data Group), Review of particle physics, Prog. Theor. Exp. Phys. **2022**, 083C01 (2022).

[91] C. O'Hare, Zenodo (2020), https://cajohare.github.io/AxionLimits/.

[92] M. Galaverni, Redshift dependent cosmic birefringence from axionlike dark matter, Proc. Sci. ICHEP2022 (**2022**) 126.

[93] A. Lewis and S. Bridle, Cosmological parameters from CMB and other data: A Monte Carlo approach, Phys. Rev. D **66**, 103511 (2002).

[94] A. Lewis, Efficient sampling of fast and slow cosmological parameters, Phys. Rev. D **87**, 103529 (2013).